



HAL
open science

Imprints of wave climate and mean sea level variations in the dynamics of a coastal spit over the last 250 years: Cap Ferret, SW France

Alphonse Nahon, Déborah Idier, Nadia Senechal, Hugues Féliès, Cyril Mallet,
Julie Mugica

► To cite this version:

Alphonse Nahon, Déborah Idier, Nadia Senechal, Hugues Féliès, Cyril Mallet, et al.. Imprints of wave climate and mean sea level variations in the dynamics of a coastal spit over the last 250 years: Cap Ferret, SW France. *Earth Surface Processes and Landforms*, 2019, 10.1002/esp.4634 . hal-02165008

HAL Id: hal-02165008

<https://brgm.hal.science/hal-02165008v1>

Submitted on 27 Jun 2019

HAL is a multi-disciplinary open access archive for the deposit and dissemination of scientific research documents, whether they are published or not. The documents may come from teaching and research institutions in France or abroad, or from public or private research centers.

L'archive ouverte pluridisciplinaire **HAL**, est destinée au dépôt et à la diffusion de documents scientifiques de niveau recherche, publiés ou non, émanant des établissements d'enseignement et de recherche français ou étrangers, des laboratoires publics ou privés.

Imprints of wave climate and mean sea level variations in the dynamics of a coastal spit over the last 250 years: Cap Ferret, SW France

Journal:	<i>Earth Surface Processes and Landforms</i>
Manuscript ID	ESP-18-0356.R3
Wiley - Manuscript type:	Research Article
Date Submitted by the Author:	n/a
Complete List of Authors:	Nahon, Alphonse; Université de Bordeaux, UMR CNRS 5805 EPOC; Bureau de Recherches Géologiques et Minières, Idier, Déborah; BRGM - French Geological Survey, DRP Sénéchal, Nadia; University of Bordeaux, UMR EPOC Féniès, Hugues; ENSEGID, Géoressources et Environnement Mallet, Cyril; BRGM - French Geological Survey, Aquitaine agency Mugica, Julie; BRGM - French Geological Survey, Aquitaine agency
Keywords:	Barrier systems, Tidal inlet, Sea level rise, NAO, Dalton Minimum

SCHOLARONE™
Manuscripts

1
2
3 1 **Imprints of wave climate and mean sea level variations in the**
4
5
6 2 **dynamics of a coastal spit over the last 250 years: Cap Ferret, SW**
7
8
9 3 **France**

10
11 4
12
13
14 5 **Alphonse Nahon^{1,2}, Déborah Idier³, Nadia Sénéchal¹, Hugues Féliès⁴, Cyril Mallet¹**
15
16 6 **and Julie Mugica¹**

17
18
19
20
21 8 ¹ University of Bordeaux, UMR EPOC, Pessac, France.

22
23 9 ² BRGM – French Geological Survey, Nouvelle-Aquitaine agency, Pessac, France.

24
25 10 ³ BRGM – French Geological Survey, Risks and prevention department, Orléans,
26
27
28 11 France.

29
30 12 ⁴ ENSEGID, Pessac, France.

31
32
33
34
35 14 Corresponding author: Alphonse Nahon (alphonse.nahon@u-bordeaux.fr)

36
37
38
39 16 **Key words:**

40
41 17 Barrier systems; Tidal inlet; Sea level rise; Climate; NAO; Dalton Minimum.
42
43
44
45
46
47
48
49
50
51
52
53
54
55
56
57
58
59
60

1
2
3 18 **Abstract**
4

5
6 19 In coastal areas, sea level rise (SLR) and changing wave climates are expected to be
7
8 20 the main oceanic drivers of shoreline adjustments. These drivers have been shown to
9
10 21 vary on a wide spectrum of spatial and temporal scales. Nonetheless, a general rule
11
12 22 about how this variability impacts global shorelines remains to be articulated. Here, we
13
14 23 discussed the impacts of wave climate changes and SLR on the evolution of a barrier-
15
16 24 spit – inlet system over the last 250 years. The distal end of the Cap Ferret barrier-spit,
17
18 25 SW France, has undergone large-scale oscillations that were well correlated with
19
20 26 variations of the decadal average of the winter North Atlantic Oscillation (NAO) index.
21
22 27 The local wave climate hindcast supports that increased alongshore wave energy fluxes
23
24 28 associated with the positive phase of the NAO were responsible for the updrift retreat of
25
26 29 the spit. In another case, the spit has elongated downdrift when waves were less
27
28 30 energetic and more shore normal, as during the negative phase of the NAO. In addition,
29
30 31 lower rates of SLR appeared necessary for the spit to develop, as higher rates of SLR
31
32 32 very likely forced the adjacent inlet to enlarge, at the expense of the spit. These results
33
34 33 should help to predict and detect coastal adjustments driven by climate change and
35
36 34 variability.
37
38
39
40
41
42
43
44
45
46
47
48
49
50
51
52
53
54
55
56
57
58
59
60

36 Introduction

37 Slower eustatic sea level rise (SLR) over the last 6 ka has allowed the formation of
38 barrier spits at the entrance of many of the world's estuaries and bays (Davis, 2013).
39 Growing barriers would then create bar-built estuaries or coastal lagoons where rich
40 ecosystems have developed. Provided that such sheltered areas remained open to the
41 sea, they have become attractive for human activities. This has added an economic
42 dimension to their ecological value and role (Newton et al., 2014). Such factors are
43 among the many reasons that continue to motivate multidisciplinary studies to improve
44 our understanding of barrier spit dynamics and their interactions with estuary and
45 lagoon entrances.

46 Where sediments are abundant, it is recognised that sort of a competition between
47 wave-driven alongshore sediment transport (LST) and estuarine (fresh and saltwater)
48 flows, controls the existence of spits as it does for inlets (FitzGerald et al., 2015; Hayes,
49 1979; Nichols and Allen, 1981). From the spit perspective, LST generally plays a
50 constructive role while flows favour inlets (Kraus, 1998; Kraus and Seabergh, 2002).

51 Inlet (cross-section) stability can be rated as good, fair or poor based on the ratio of the
52 spring tidal prism by the total littoral drift (Bruun, 1978). Larger freshwater inputs
53 ultimately favour inlet stability as confirmed by numerical modelling (Zhou et al., 2014).

54 These forces vary as waves, sea level and rainfalls change with seasons and climate
55 shifts. In mixed-energy environments (Hayes, 1979), such variability can lead to
56 noticeable changes of local morphology. Such changes may occur fortnightly, as it does
57 for small systems (Fortunato et al., 2014), and at any larger timescale at which driving
58 forces may change. For instance, if most barrier spits were able to build during periods

1
2
3 59 with relatively low rates of sea-level rise (SLR), questions remain about how they would
4
5
6 60 respond to predicted higher rates of SLR and changing wave climate for the coming
7
8 61 decades (Cazenave and Le Cozannet, 2014; Semedo et al., 2013).

9
10 62 There is indeed a persistent and immediate need to improve the prediction of climate
11
12 63 change impacts on coastal systems worldwide (Wong et al., 2014). Main drivers include
13
14 64 SLR, the alteration of rainfall and runoff and changing wave climates which are crucial
15
16
17 65 for spits and inlets' evolution (Ranasinghe et al., 2012). In most coastal embayments,
18
19 66 SLR leads to larger values of tidal prisms that force inlets to increase their cross-section
20
21 67 (FitzGerald et al., 2008). In places with low continental sediment inputs, SLR would also
22
23 68 create accommodation space in embayments that may become sediment sinks for the
24
25
26 69 adjacent coasts (Ranasinghe et al., 2012). Where freshwater runoff contributes to
27
28 70 maintain inlets, it may also cause adjacent spit retreat or progradation as rainfall
29
30
31 71 respectively increases or diminishes (Ranasinghe et al., 2012). Finally, changing storm
32
33 72 tracks, storm intensity and frequency are likely to modify coastal resilience (Masselink et
34
35 73 al., 2016) and have a direct impact on the wave driven LST (Chowdhury and Behera,
36
37 74 2017; Splinter et al., 2012).

38
39
40 75 Along with natural climate variability, these drivers have already varied over a wide
41
42 76 range of temporal and spatial scales. At inter-annual to decadal timescales,
43
44 77 atmospheric teleconnection patterns, such as the North Atlantic Oscillation (NAO), and
45
46 78 climatic cycles such as the El Niño Southern Oscillation (ENSO) over oceanic basins
47
48 79 have remote effects on coastal environments (Barnard et al., 2011; Masselink et al.,
49
50 80 2014; Wiggins et al., 2017). On longer timescales, the stratigraphic records of coastal
51
52 81 barrier spits have also revealed the control exerted by sea level changes (Clemmensen
53
54
55
56
57
58
59
60

1
2
3 82 et al., 2001; Fruergaard et al., 2015) and major storm events (Fruergaard et al., 2013).
4
5 83 This climate-driven variability can overlay the system internal cyclicality and play a part in
6
7 84 rhythmic behaviours that are common along barrier coasts (Allard et al., 2008;
8
9 85 Ridderinkhof et al., 2016). These cycles have substantial effects on shoreline dynamics.
10
11 86 Nonetheless, due to limited number of detailed geomorphological datasets, on the
12
13 87 longer term it is often unclear whether cyclicality is driven by the system intrinsic nature
14
15 88 (i.e., autocyclic) or by external (climatic) factors (i.e., allocyclic).
16
17 89 On the other hand, global knowledge on climate variability and its effects is constantly
18
19 90 growing. Coupled ocean-atmosphere numerical models help to describe processes
20
21 91 underlying relationships between parameters of different nature as, for instance, sea
22
23 92 level pressure, anomalous coldness and storm tracks (van der Schrier and Barkmeijer,
24
25 93 2005), solar irradiance and teleconnection patterns (Ineson et al., 2011) or
26
27 94 teleconnection patterns and sea level (Calafat et al., 2012). Going back to interactions
28
29 95 between barrier spits and inlets, recent studies address the impact of climate change
30
31 96 through the application of process-based morphodynamic models to tidal embayments
32
33 97 (Bruneau et al., 2011; Dissanayake et al., 2012; van Maanen et al., 2013; van der
34
35 98 Wegen, 2013). Those studies primarily discuss the effects of SLR and describe the
36
37 99 evolution of the sediment source-to-sink nature of inlets over time. Such growing
38
39 100 understanding of both the dynamic nature of climate and of the processes changing the
40
41 101 coastal landscape widens the spectrum of possibilities for interpreting documented
42
43 102 coastal evolutions.
44
45 103 This study thrives on these possibilities to discuss the coherence between large-scale
46
47 104 coastal changes and variable environmental conditions. The next section presents a
48
49
50
51
52
53
54
55
56
57
58
59
60

1
2
3 105 dataset with outstanding temporal coverage and resolution. It covers the morphological
4
5 106 evolution of the Cap Ferret sand spit (SW France, Atlantic coast) over the last 250 years
6
7 107 and contemporaneous environmental conditions. Then section 3 investigates the
8
9 108 synchronisation of the apparent cyclical dynamic of the spit distal end with climatic shifts
10
11 109 and sea level variations. Potential mechanisms underlying this synchronisation are
12
13 110 subsequently discussed based on current understanding of barrier spits and tidal inlets
14
15 111 morphodynamics, allowing to identify the dominant climatic drivers (section 4).
16
17
18
19
20
21

22 113 **Materials and methods**

23 24 114 ***Study area***

25
26 115 The Cap Ferret is a baymouth spit bordered by the Bay of Biscay (Figure 1). It lies at
27
28 116 the southern end of a 110 km long uninterrupted sandy beach bounded by the Gironde
29
30 117 estuary to the north (Aubié and Tastet, 2000; Castelle et al., 2018; Figure 1b). The
31
32 118 subaerial fraction of the spit accounts for the beach last twenty kilometres and is built
33
34 119 upon a subtidal platform that dips into the Bay of Arcachon tidal inlet (Figure 1c). This
35
36 120 inlet connects a 160 km² coastal lagoon to the Atlantic Ocean, the lagoon – inlet system
37
38 121 being the vestige of the Leyre River estuary (Féniès and Lericolais, 2005). Around 3 *ka*
39
40 122 ago the Cap Ferret started to build up on the estuary northern margin (Féniès et al.,
41
42 123 2010), pushing the river mouth southward until it semi-enclosed the Bay of Arcachon.
43
44 124 At present, water circulation between the lagoon and the ocean constricts the spit
45
46 125 progradation. Twice a day between 260 and 490 Mm³ of water flow in and out through
47
48 126 the inlet, confirming that at any time tidal exchanges largely take over on freshwater
49
50 127 inputs (Plus et al., 2009). Such high values of tidal prism (P) largely overcome the total
51
52
53
54
55
56
57
58
59
60

1
2
3 128 LST (M), estimated at 0.661 Mm³ (Idier et al., 2013), so that this opening falls into the
4
5 129 “good stability” category ($P/M \gg 150$) of (Bruun, 1978) classification. Nonetheless,
6
7
8 130 northwesterly dominant waves have deviated the estuary mouth some thirty kilometres
9
10 131 downdrift in the past 3 *ka* (Féniès et al., 2010). Annual mean significant wave height is
11
12 132 of 1.77 m (in 50 m water depth, according to Charles et al., 2012) and mean tidal range
13
14 133 is of 2.7 m (twice the semidiurnal tidal component amplitude, measured on the ebb-
15
16
17 134 delta’s shield, by Senechal et al., 2013). This mixed-energy environment, as defined by
18
19 135 Hayes (1979), has moulded an inlet with a transitional morphology (Hubbard et al.,
20
21 136 1979). The inlet ebb-tidal delta is more developed than the flood-tidal shoals (Figure
22
23
24 137 1c). This disequilibrium reflects the ebb dominance confirmed by morphodynamic
25
26 138 modelling (Cayocca, 2001). Model results further showed the role of the ebb-dominant
27
28 139 tide in the breaching of new channels across the spit platform. Indeed, historical charts
29
30
31 140 report various occurrences of the formation of a new channel across the platform. Over
32
33 141 the last 300 years, newly opened channels have migrated southward and the detached
34
35 142 shoals ultimately reached and merged to the inlet southern margin, in a movement that
36
37
38 143 resembles the spit-platform breaching model of sediment by-passing of FitzGerald et al.
39
40 144 (2001). The apparent cyclical nature of this process has led to the hypothesis of an 80-
41
42 145 year autocyclic behaviour. According to charts, the inlet has been alternatively
43
44
45 146 composed of one or two channels and Michel and Howa (1997) further interpreted the
46
47 147 retreat of the subaerial fraction of the spit as a feedback from the breaching of new
48
49 148 (secondary) channels. However, a thorough discussion of the role of variable
50
51 149 environmental conditions is still lacking. The premises of such a discussion were given
52
53
54 150 by Nahon et al. (2015). In this first analysis, it was noted that the autocyclic model fails

1
2
3 151 to predict a major spit progradation event. Instead, spit elongation was found
4
5 152 synchronous with periods dominated by the negative phase of the NAO.
6
7 153 The present study builds upon Nahon et al. (2015) data to further infer on the role that
8
9 154 climate and SLR may have played in inlet – spit interactions. Cap Ferret is well suited
10
11 155 for this study because of 3 reasons: 1) updrift sandy beaches prevent from any
12
13 156 sediment deficit; 2) it is backed up by a mature estuary where an elevated level of
14
15 157 infilling makes tidal prism sensitive to mean sea level variations; 3) the first
16
17 158 quantitatively valuable chart dates from 1768 and the evolution of the spit-inlet system
18
19 159 can be reconstructed over the last 2.5 centuries.
20
21
22
23
24
25

26 161 **Shoreline data**

27
28 162 The geomorphological record encompasses the entire 19th and 20th centuries and
29
30 163 consists of nautical charts and aerial photographs of the Bay of Arcachon's tidal inlet
31
32 164 (Figures 2 to 4).

33
34 165 Charts were retrieved from Caspari (1872), Lapeyre (1925) and Bordeaux harbour
35
36 166 authorities (PAB, 1985). All made appear 3 reference positions on charts (Figure 2): the
37
38 167 still existing Cap Ferret's lighthouse and the church *Notre-Dame d'Arcachon*, both
39
40 168 located north of the spit distal end, and a former semaphore on the southern margin.
41
42 169 This later position was retrieved from the map of the Gironde department in 1888
43
44 170 (Figure 2a). These positions were used for georeferencing.

45
46 171 Clear and stable features along the spit were used to estimate the error on the charts
47
48 172 before 1900. Preserved former spit-end positions and small bights on the lagoon side of
49
50 173 the spit, indicate a distance error well below 200 m. Therefore, a +/- 200 m error bars
51
52
53
54
55
56
57
58
59
60

1
2
3 174 marks off the results to avoid any misinterpretation. Early 20th century charts also
4
5 175 indicate a (still existing) semaphore located 1 km north of the 2014 shoreline. The root
6
7 176 mean square error for the semaphore positions is 55 m and results are also shown with
8
9
10 177 +/- 100 m error bars to account for possible shoreline misinterpretation at the time of the
11
12 178 survey. The spit terminus was then defined as the southernmost position of the
13
14 179 coastline represented on charts (Figure 3). These positions were orthogonally projected
15
16
17 180 onto the axis defined by 2 of the reference positions used for georeferencing nautical
18
19 181 charts (Figure 3).
20
21 182 Positions measured on charts from 1932 and 1936 presented a very good match with
22
23 183 those on photographs from 1934 and 1946 respectively (Figure 4). Between 1934 and
24
25 184 2000, aerial photographs were used. They were georeferenced using the current road
26
27 185 and pathway network and, at some point, World War II bunkers on top of the dunes.
28
29 186 After 2000, 7 high resolution orthophotomaps were used. Georeferencing errors are
30
31 187 lower than the shoreline photo-interpretation error that was estimated well below +/- 50
32
33 188 m. On photographs, the southernmost position of the interpreted shoreline (i.e. berm
34
35 189 crest when perceptible, high-tide wrack line otherwise) was taken to measure the spit
36
37 190 extension. Overall, 50 positions of the Cap Ferret distal end were retrieved since 1768
38
39 191 (24 on charts from 1768 to 1936, Figure 3; 26 on photographs from 1934 to 2014,
40
41 192 Figure 4). These positions were used to trace the path of the spit distal-end. In the
42
43 193 following, periods over which the spit advanced across the inlet were identified from this
44
45 194 path. Still, it is a limited indicator of erosion or accretion patterns as it does not consider
46
47 195 the behaviour of the spit in the direction perpendicular to the reference axis.
48
49
50
51
52
53
54 196
55
56
57
58
59
60

197 ***Bathymetric data***

198 Shoreline data document north-south oscillations of the spit distal end, the last large-
199 scale oscillation occurring between 1950 and 2014 (Figure 4). Over this period,
200 bathymetric evolution of the adjacent inlet throat was quantified using soundings from
201 years 1949, 1969, 1979, 2001 and 2014.

202 Over the years, along transect resolution increased from 100 m to 1 m and transect
203 positioning and spacing (~200m) remained constant (Figure 5a). For each survey,
204 transects have been interpolated into digital elevation models (DEMs); 50 m x 50 m
205 surfaces were created using a nearest-neighbour interpolation (Figure 5b). Bottom
206 elevation and volumetric changes were computed over a 12.74 km² overlapping surface
207 between all 5 DEMs. Figure 5d presents the erosion-deposition patterns over the 65
208 years.

209 A distinction was made between shoals and channels using the -7 m NGF contour
210 (NGF is the French vertical datum; locally Mean Sea Level is currently around +0.40 m
211 NGF). This contour match well with shoals visible on contemporary Landsat 8 image
212 (Figure 5c). For each date, 4 quantities were computed. The first 3 are the mean
213 elevation and the shoal and channel volumes which are respectively the sand volume
214 above -7 m NGF and water volume below -7 m NGF. As little to none information exists
215 to estimate errors due the instrumental bias or vertical datum changes over time (others
216 than the known and corrected ones), a fourth quantity, defined as the inlet throat
217 *morphological amplitude* was calculated. It corresponds to the equal volumes of sand
218 and water, respectively above and below the mean elevation of each DEM. In this way,
219 this later quantity is free of any artificial variations. Results are summarised in Table 1.

1
2
3 220 Figure 5 (e-h) further presents the variation of the computed quantities with the
4
5 221 identified periods of elongation and retreat of the spit-end.
6
7
8 222

9
10 223 **Sea level data**

11
12 224 To infer on the role of sea level variations in the evolutions depicted by cartographic and
13
14 225 bathymetric data, the annual mean sea level (MSL) record from Brest tidal gauge
15
16 226 (Figure 1) was retrieved from the permanent mean sea level observatory (Holgate et al.,
17
18 227 2013); it is the nearest tidal gauge with an appropriate temporal coverage (Wöppelmann
19
20 228 et al., 2008). Over the entire period the data is fitted to a 2nd order polynomial function
21
22 229 which reveals the lowering of MSL during the first third of the 19th century (Figure 6,
23
24 230 upper panel). Then over the 20th century, the data is both averaged and fitted to a
25
26 231 polynomial function. The running mean over an 11-year-centred window is used to
27
28 232 emphasise the significant decadal variability of the regional MSL. Then, fitting the record
29
30 233 with 5th order polynomial function allows identifying a period of slower SLR around the
31
32 234 second third of the 20th century (Figure 6, lower panel).

33
34 235 Table 2 further indicates average SLR rates over identified periods of spit growth and
35
36 236 decay. Rates are computed as the linear trend in the overlapping sea level data. The
37
38 237 overlap is defined by adding sea level data until preceding and following spit-end
39
40 238 positions to the actual identified period (excepted for 1909 because of the important 20-
41
42 239 year interval between positions). This lengthens the periods over which the trend is
43
44 240 computed. When computed over the exact (shorter) intervals, differences between
45
46 241 successive periods of growth and decay are more pronounced.
47
48
49
50
51
52
53

54 242
55
56
57
58
59
60

243 **Wave climate data**

244 To assess the impact from variations of wave-driven forces, the local wave climate
 245 during the last oscillation of the spit-end was characterized by means of a hindcast
 246 simulation, performed with the storm surge modelling system of Bertin et al. (2015). The
 247 model was extended to the whole North Atlantic Ocean and forced with wind fields
 248 originating from the NCEP/NCAR reanalysis (Kalnay et al., 1996), over the period 1949-
 249 2014. Hindcasted wave parameters were validated against measurements from a
 250 directional wave buoy moored in 54 m water depth, and located 15 km offshore the
 251 study site (CETMEF, n.d.). Between 2007 and 2014, 92602 measurements,
 252 representative of 5.3 years in record length, were compared to interpolated modelled
 253 parameters. For both modelled and measured parameters, the wave power (WP) is
 254 approximated with the linear wave theory (Svendsen, 2006; Eq. 1-2), as the wave
 255 energy (E) times the wave group velocity (c_g), after computing the phase velocity (c)
 256 using an iterative method to solve the dispersion relationship for calculating (in
 257 intermediate water depth) the wave number (k) associated with the peak angular
 258 frequency (ω).

260 Eq. 1: $WP = Ec_g$

261 Eq. 2: $E = \frac{1}{8}\rho g H_s^2; c_g = c * \frac{1}{2} \left(1 + \frac{2kh}{\sinh 2kh}\right); c = \frac{\omega}{k}$

262
 263 The WP is then decomposed into cross-shore (WP_x) and alongshore (WP_y) energy flux,
 264 positive when landward and northward respectively. Table 3 summarizes the
 265 comparison outcomes for the significant wave height (H_s), the WP and mean wave

1
2
3 266 energy direction ($wDir$), computed with mean WP_x and WP_y . Modelled and observed
4
5 267 parameters are in good agreements. Pearson linear correlation coefficient are equal to
6
7 268 0.93 and 0.80 for respectively WP and WP_y and the modelled wave field only slightly
8
9 269 underestimating the total WP by 2.4%. In terms of direction, $wDir$ has an initial bias of
10
11 270 3.8° . After removing the bias, correlation between modelled and observed WP_y is
12
13 271 improved to 0.81 and the error on averaged WP_y is minimal (1.7%). Low-pass filtered
14
15 272 WP and WP_y on Figure 7 further reveal the good performance of the model, as
16
17 273 correlation coefficients grow to 0.99 and 0.95 for WP and WP_y respectively.
18
19
20
21
22 274

23 24 275 **North Atlantic Oscillation (NAO)**

25
26 276 Over the entire period covered by geomorphological data, winter indices of the North
27
28 277 Atlantic Oscillation (NAO) provide additional information about the environmental
29
30 278 forcing. The NAO is the main atmospheric mode of variability over the North Atlantic
31
32 279 basin in winter (Hurrell and Deser, 2009), and from December to March, its negative
33
34 280 and positive phases have a demonstrated influence on ocean waves and sea level
35
36 281 anomalies on Western Europe coastlines (Calafat et al., 2012; Dodet et al., 2010).
37
38 282 Therefore, 3 different NAO indices were used as proxy for these environmental drivers.
39
40 283 Indices of the winter NAO in the literature are either reconstructions based on a
41
42 284 combination of instrumental and proxy data (Cook et al., 2002; Glueck and Stockton,
43
44 285 2001; Luterbacher et al., 1999; Ortega et al., 2015), indices computed from the
45
46 286 difference of normalized sea level pressure between the Azores High and the Icelandic
47
48 287 Low (Hurrell, 1995; Jones et al., 1997), or indices based on a principal component
49
50 288 analysis of reconstructed sea level pressure fields over the North Atlantic Ocean
51
52
53
54
55
56
57
58
59
60

1
2
3 289 (Barnston and Livezey, 1987; Hurrell, 2019). This study used the station-based index of
4
5 290 Hurrell (2015) which provides empirical evidence until 1864. This record is extended
6
7 291 back to 1768, with two proxy-based reconstructions selected for their robustness
8
9
10 292 against this instrumental data (Luterbacher et al., 2001; DJFM index, accessed from
11
12 293 <https://www.ncdc.noaa.gov/paleo-search/study/6275>) and their novelty (Ortega et al.,
13
14 294 2015; DFJ index, accessed from <https://www.ncdc.noaa.gov/paleo-search/study/18935>).
15
16
17 295 In the following, these indices are either showed in their cumulative form or as decadal
18
19 296 averages. To highlight the dominance of either the negative or positive phase of the
20
21 297 NAO in winter, cumulative indices were computed. After Mazzarella and Scafetta
22
23 298 (2012), the cumulative value of each index for a given year is taken as the inclusive sum
24
25
26 299 of values for all previous years. Then over the 20th century onward, more frequent spit-
27
28 300 end positions are compared to the station-based index, averaged over the 10 years
29
30
31 301 preceding each observation. This averaging procedure was needed because of the
32
33 302 irregularly sampled observations; the 10-year window was found to fit well with this
34
35 303 irregular resolution and the inertia of the system compared to the high interannual
36
37 304 variability of the NAO (Hurrell, 1995).
38
39
40 305

306 **Results and basis for discussion**

307 ***Three periods of spit lengthening***

308 Upper panel in Figure 8 represents the path of the Cap Ferret spit-end from 1768 to
309 2014; lower panels show cumulated NAO indices. The spit-end path reveals 3 periods
310 over which the spit has dominantly grown across the inlet. These periods, over 40 years
311 each, are delimited by local extrema of the spit-end position, on maps and photos of

1
2
3 312 1768-1826, 1865-1909 and 1932-1972. The 1st and 3rd periods are found when the
4
5 313 negative phase of the NAO has dominated (Figure 8, lower panels). Likewise, according
6
7 314 to the station-based index (Hurrell, 2015), the negative phase of the NAO has
8
9 315 dominated during most of the 2nd period, until 1902, or 7 years before the map of 1909.
10
11
12 316

14 317 ***The Dalton Minimum***

16
17 318 The 1st period of spit lengthening, characterized by a 3.5 km lengthening of the spit
18
19 319 between 1805 and 1826, was also contemporaneous with the Dalton Minimum (DM,
20
21 320 1780-1830) climate anomaly. Figure 9 details this record lengthening and the
22
23 321 subsequent retreat. The spit has grown while the tidal inlet had 2 well defined channels.
24
25 322 Both northern and southern channels were preserved as the spit grew, but the inlet
26
27 323 minimal width was divided by 3 in 1826 compared to that of 1768. Then between 1826
28
29 324 and 1865, the spit has retreated while the inlet width regained a width comparable to its
30
31 325 1768 level. In 1865 the southern channel was buried by the main inlet shoal that have
32
33 326 steadily migrated southward since 1768 attached to the inlet's southern margin.
34
35 327 Therefore, during a century, the spit has advanced against a double channelled inlet
36
37 328 and has retreated when the inlet's southern channel closed. In terms of climate, this
38
39 329 century encompassed the Dalton Minimum which was a period of anomalous coldness
40
41 330 (van der Schrier and Barkmeijer (2005) and references therein).
42
43 331 DM is explained as a conjunction of low solar activity and major volcanic eruptions and
44
45 332 has culminated in Europe with "the year without a summer" in 1816 (van der Schrier and
46
47 333 Barkmeijer, 2005). Using a global circulation model, van der Schrier and Barkmeijer
48
49 334 (2005) have pointed out the "higher occurrence probability at the European mid-
50
51
52
53
54
55
56
57
58
59
60

1
2
3 335 latitudes of the strongest cyclone under DM atmospheric conditions”. Their results recall
4
5 336 those from Shindell (2001) and Ineson et al. (2011), who showed that periods, or years,
6
7 337 with low solar activity produce NAO negative like atmospheric configurations. Indeed,
8
9 338 during the negative phase of the NAO low pressure systems are deviated southward
10
11 339 (Hurrell and Deser, 2009). Furthermore, there is converging evidence of enhanced mid-
12
13 340 latitude storminess during such cold periods, as recorded by the dune fields north and
14
15 341 south of Cap Ferret (Clarke et al., 2002).

16
17 342 The dominance of the negative phase of the NAO during DM is also suggested by the
18
19 343 cumulative NAO winter-index of Luterbacher et al. (2001), that decreased until 1830
20
21 344 (Figure 8, mid panel). However, as recalled by Poirier et al. (2017), NAO reconstruction
22
23 345 tend to diverge in this period. For instance, the data from Ortega et al. (2015) only
24
25 346 confirm Luterbacher’s data until 1810 when, according to the more recent
26
27 347 reconstruction, the positive phase begins to dominate again. On the other hand, when
28
29 348 compared to the station-based index computed by (Hurrell, 2015) from the instrumental
30
31 349 record, Luterbacher’s reconstruction performs better. Indeed, Luterbacher’s (DJFM)
32
33 350 reconstruction is well correlated with the station-based index from 1864 onward (Figure
34
35 351 8 mid panel), while the correlation between Ortega’s (DJF) reconstruction and
36
37 352 instrumental data between 1864 and 1969 is weaker (Figure 8 lower panel); Pearson
38
39 353 linear correlation coefficient (r) equal to 0.89 (p -value $< 10^{-47}$) in the first case, against a
40
41 354 correlation coefficient of 0.47 (p -value $< 10^{-6}$) in the second case.
42
43
44
45
46
47
48
49
50

355

51 356 ***Correlation with NAO winter-indices***

1
2
3 357 After the DM, the other 2 periods of spit growth happened while the negative phase of
4
5 358 the NAO have dominated in winter, as supported by Hurrell's (2015) station-based index
6
7 359 (Figure 8, middle panel). By opposition, periods of spit retreat systematically took place
8
9
10 360 in periods dominated by the positive phase of the winter NAO; on Figure 8, periods
11
12 361 delimited by the local extrema of the spit-end position, on maps and photos of 1826-
13
14 362 1865, 1909-1932 and 1972-2014.

15
16
17 363 Over the 20th century, sharp movements of the spit-end like those around 1915 and
18
19 364 1972 were also synchronous with remarkable shifts of the NAO (Figure 10, upper
20
21 365 panel): between 1909 and 2000, the spit-end path is significantly correlated with the
22
23 366 decadal average of the NAO winter-index ($r = -0.67$, $p\text{-value} < 10^{-4}$).

24
25
26 367 Locally, the positive phase of NAO is known to produce higher and more oblique
27
28 368 (clockwise shift) winter waves (Charles et al., 2012). The hindcast used in this study
29
30 369 agrees with this and further shows how decadal averages of the winter NAO index and
31
32 370 the alongshore wave power are well correlated (Figure 10, lower panel; $r = 0.86$, $p\text{-value}$
33
34 371 $< 10^{-16}$). Correlation is greater than for the total wave power (WP), which has a
35
36 372 correlation coefficient of 0.76 ($p\text{-value} < 10^{-11}$). This highlights the impact of the NAO on
37
38 373 the local wave direction as well. Consequently, according to wave climate between
39
40 374 1949 and 2014, decades dominated by the positive phase of the NAO may produce an
41
42 375 average alongshore wave power up to 30% greater than when the negative phase
43
44 376 dominates (figure 10, lower panel).

45
46
47 377 Nonetheless, although winter wave power and NAO index remain correlated until 2014,
48
49 378 their apparent relationship with the spit-end track is less clear at the beginning of the
50
51
52
53
54
55
56
57
58
59
60

1
2
3 379 21st century. Since 2000, averaged wave power and NAO index have regained a more
4
5 380 neutral value while the spit have continued to retreat.
6
7

8 381

9
10 382 ***Sea level and inlet width variations***

11
12 383 The ongoing erosion and retreat of the spit-end comes after the last significant
13
14 384 lengthening which has culminated in 1972 (Figures 4 & 10). In addition to a dominant
15
16 385 negative phase of the NAO in winter (Figures 8 & 10), the spit has then advanced
17
18 386 across the inlet while, since the 1930s, sea level was rising at a relative slow pace (1.26
19
20 387 mm.y⁻¹) compared to that of the beginning and end of the 20th century (above 2.4 mm.y⁻¹
21
22 388 1; see Table 2 and Figure 6 lower panel). During this period, the inlet channel volume
23
24 389 and the morphological amplitude of the inlet throat were also relatively stable or slightly
25
26 390 decreased (Figure 5).
27
28

29
30
31 391 Around 1972, the spit-end growth was sharply interrupted. In the same time the
32
33 392 morphological amplitude of the inlet throat remained stable until 1979. Instead, as the
34
35 393 winter NAO abruptly shifts towards the dominance of the positive phase, the decadal
36
37 394 averaged of the alongshore wave power increased and reached its highest level
38
39 395 between 1970 and 1990. It is only after 1979 that the inlet channel volume has begun to
40
41 396 increase, synchronous with an acceleration of sea level rise (Figure 6). Since then
42
43 397 channel volume has increased over 25%, while the wave energy remains at an average
44
45 398 level.
46
47

48
49 399 The increase in channel volume recalls the dramatic expansion of the inlet observed
50
51 400 after 1826 (Figure 9). This first *breathing* then occurred as sea level has successively
52
53 401 fallen and risen (Table 2). In the absence of detailed analysis of the evolution of the
54
55
56
57
58
59
60

1
2
3 402 inlet's dimensions over the second period of spit lengthening, linear trends presented in
4
5 403 Table 2 reveal that for all 3 periods of spit lengthening, sea level has either fallen or has
6
7
8 404 risen slower than during preceding and following periods.
9
10
11
12
13
14
15
16
17
18
19
20
21
22
23
24
25
26
27
28
29
30
31
32
33
34
35
36
37
38
39
40
41
42
43
44
45
46
47
48
49
50
51
52
53
54
55
56
57
58
59
60

For Peer Review

405 **Discussion**

406 ***The auto-cyclic hypothesis***

407 From the 1960s to until recently (2014), the present set of maps and photos has been
408 gathered and analysed numerous times by several authors, mainly for engineering
409 purposes (see Nahon, 2018, for references). The main idea which raised is that Cap
410 Ferret's spit-end north-south oscillations could be an auto-cyclic response to the
411 apparent cyclicity of the inlet channel configuration (with one or two channels). Michel
412 and Howa (1997) detailed the cyclical nature of the inlet channels and conceptualized
413 its impacts on the inlet's northern and southern margins. Among other impacts, their
414 conceptual model predicts that the Cap Ferret spit extends southward when a single
415 channel exists and by opposition retreats when two channels split the inlet. This
416 feedback interaction was derived from approximately the same cartographic data
417 presented in here. However, such hypothesis is far less than evident during over a third
418 of the data coverage. Indeed, as shown in Figure 9, let's recall here that between 1769
419 and 1825, the spit has elongated while the inlet had two channels and that from 1825 to
420 1865, the spit has retreated when the southern channel was progressively buried. On
421 the other hand, there is an apparent relationship between the spit-end behaviour and
422 the North Atlantic climate over the entire study period.

424 ***Wave climate influence***

425 Links between the NAO and the local wave climate could be part of the explanation to
426 the spit – climate apparent relationship. Indeed, it appears that the spit grows across the
427 inlet when NAO-negative ocean waves are more shore normal and/or the alongshore

1
2
3 428 wave power is below average. By opposition, the spit-end retreats when the alongshore
4
5 429 wave power is stronger than average, and as so when the wave-driven alongshore
6
7 430 sediment transport (LST) is more intense. Aagaard et al. (2004) have observed a similar
8
9 431 relationship along the western Danish coast in northern Europe. Based on wind data
10
11 432 from the first and last 30 years of the 20th century, they have pointed out the contribution
12
13 433 of increased wind-wave driven LST, to the updrift erosion of the spit-end towards the
14
15 434 end of the century. More recently, Aagaard and Sørensen (2013) have suggested the
16
17 435 increase of the LST surpasses all terms in the sediment *imbalanced* equation, including
18
19 436 sea-level rise. Underlying physical processes are yet to be identified, however they
20
21 437 could either lie within LST – inlet flow interactions (Bertin et al., 2009), or within wave
22
23 438 orientation – spit-growth relationship (Ashton et al., 2016).
24
25
26 439 On the one hand, Bertin et al. (2009) have shown with a process-based morphodynamic
27
28 440 model, that sediment retention within tidal inlets could increase when waves approach
29
30 441 the coast at a lower angle of incidence; therefore when, to all other parameters equal,
31
32 442 LST is reduced. Locally, this is quite meaningful because the nonlinear superimposition
33
34 443 of the southward LST induced waves and tidal residuals increase alongshore gradients
35
36 444 in sediment transport (Cayocca, 2001).
37
38
39 445 On the other hand, simulations with coastal evolution models (CEM) suggest that the
40
41 446 sole relationships between spit growth and wave orientation may also be at play
42
43 447 (Ashton et al., 2016): less oblique waves (and a decreased LST) leads to the erosion of
44
45 448 the spit on the updrift side of the fulcrum point and to the lengthening of spit distal end
46
47 449 (Figure 11a), whereas increasing the wave incidence and the LST induces sediment
48
49 450 retention updrift of the fulcrum point while the spit-end loses sediment and retreats
50
51
52
53
54
55
56
57
58
59
60

1
2
3 451 (Figure 11b). This apparent oscillation of the sediment budget around the fulcrum point
4
5 452 recalls the behaviour of the Cap Ferret between 1826 and 1865 (Figures 9 & 11c).
6
7 453 These examples provide some insights on the physics underlying the apparent
8
9 454 relationship between local geomorphology and local waves. Increased LST and more
10
11 455 oblique waves during the positive phase of the NAO may well have forced the spit-end
12
13 456 to retreat, while the spit can advance across the inlet when the negative phase of the
14
15 457 NAO produce waves with a reduced angle of incidence and lower rates of LST.
16
17 458 From a regional perspective, this behaviour differs from that of the Arçay sandspit (less
18
19 459 than 250 km north of Cap Ferret). Allard et al. (2008) first suggested the rhythmic
20
21 460 growth of Arçay sandspit was boosted by LST, and Poirier et al. (2017) further put into
22
23 461 evidence the hierarchical control of the NAO and the East Atlantic–West Russia pattern.
24
25 462 In the case of Arçay, higher rates of LST during the positive phase of the NAO are
26
27 463 found to be responsible for the enhanced spit growth. Here we found it is the opposite at
28
29 464 Cap Ferret. Therefore, the attempt by Poirier et al. (2017) to, in a second time,
30
31 465 associate both spits behaviour is questionable. The reason may be the important
32
33 466 difference of their back-barrier lagoon dimensions, which in the case of Arçay is a lot
34
35 467 smaller. In the case of Cap Ferret, the large lagoon of the Bay of Arcachon engenders a
36
37 468 large tidal prism that has shaped large inlet shoals. Then, the repartition of wave-driven
38
39 469 sediment inputs, between the spit and the shoals, become more complex (Hoan et al.,
40
41 470 2011; Kraus, 2000; Larson et al., 2007). This is particularly true when relative sea levels
42
43 471 are subject to rise, ultimately turning shoals into sediment sinks because their
44
45 472 equilibrium volume increases with the larger value of tidal prism engendered by higher
46
47 473 sea level (Walton, Jr. and Adams, 1976). Also, wave climate variations alone may not
48
49
50
51
52
53
54
55
56
57
58
59
60

1
2
3 474 fully explain inlet constrictions and expansions such as those observed during and after
4
5 475 the Dalton Minimum (Figure 2c-d), or the ongoing inlet throat expansion since 1979
6
7
8 476 (Figure 5).

9
10 477 ***Sea level influence***

11
12 478 A tidal inlet's cross-section increases with tidal prism (O'Brien, 1931) and, to a lower
13
14 479 degree, decreases with wave energy (Jarrett, 1976; Nahon et al., 2012). Tidal prism
15
16
17 480 variations could then have contributed to observed changes in inlet dimensions. For
18
19 481 instance, in 1990s when the wave energy is maximal (Figure 10, lower panel), only an
20
21 482 increase of the tidal prism could have caused the inlet to enlarge (Figure 5e). In
22
23 483 addition, the magnitude of the inlet's narrowing and widening in the first half of the 19th
24
25 484 century (Figure 9) suggests that changes in the tidal prism have certainly added to the
26
27 485 effects of variations of the wave climate associated with the Dalton Minimum. Over the
28
29 486 study period, the Bay of Arcachon's contours remained stable. Instead, variations of the
30
31 487 sea level must have modulated tidal prism.

32
33
34 488 Tidal flats and salt marshes occupy about 75 % of the Bay of Arcachon (Féniès and
35
36 489 Faugères, 1998; Nahon, 2018), so that the tidal prism is mostly controlled by the relative
37
38 490 elevation of those. Due to low sediment input from freshwater streams, the
39
40 491 sedimentation rate above these tidal flats is expected to respond, at most, with a
41
42 492 temporal lag to changes in the rate of sea level variations (Kirwan and Murray, 2008).
43
44 493 So that when sea level starts to increase or when sea level rise (SLR) accelerates, tidal
45
46 494 flats' relative elevation decreases temporarily, leading to a greater tidal prism that
47
48 495 ultimately forces the inlet to enlarge. On the contrary, inlets may narrow in response to
49
50 496 falling sea level or stable to decelerating SLR.
51
52
53
54
55
56
57
58
59
60

1
2
3 497 Part of the explanation would also be related to the ongoing morphological evolution
4
5 498 whole barrier system. Indeed, the large tidal flats of the lagoon and the relatively high
6
7 499 tidal range promote the ebb dominance of the system (Fortunato and Oliveira, 2005;
8
9
10 500 Friedrichs and Aubrey, 1988). The overall negative sediment budget of the lagoon
11
12 501 between charts of 1865 and 2001 (Allard et al., 2009) confirmed this characteristic.
13
14 502 Charts further revealed that sediment loss was due to headward erosion of its tidal
15
16 503 channels which, according to process-based models, can be a response of an inlet –
17
18 504 lagoon system to SLR (van Maanen et al., 2013). This similitude between simulated
19
20 505 morphologies and the observed evolution of the lagoon, suggests the Bay of Arcachon
21
22 506 is currently adapting to secular regional SLR (Jevrejeva et al., 2014). Van Maanen et al.
23
24 507 (2013) numerical experiments further explain how, under progressive SLR, such
25
26 508 systems can remain ebb-dominated and how the amount of exported sediment
27
28 509 increases with the rate of SLR.
29
30
31
32
33 510 Therefore, multiple processes could explain how decadal to pluri-decadal variations in
34
35 511 the rate of SLR (Jevrejeva et al., 2014), like those observed at Brest (Figure 6 and
36
37 512 Table 2), must have impacted the inlet sediment budget, at temporal scales matching
38
39 513 those of documented spit-end oscillations.
40
41
42
43
44
45
46
47
48
49
50
51
52
53
54
55
56
57
58
59
60

515 ***Other influences***

516 In winter, the NAO also modifies effective rainfalls and wind regimes as well as sea
517 level anomalies (Calafat et al., 2012). Locally, NAO-positive winters tends to be drier
518 (Hurrell and Deser, 2009), so that freshwater inputs to the lagoon are expected to be
519 further reduced. Therefore, it is very unlikely that the impact of the NAO on precipitation

1
2
3 520 could contribute to the observed inlet breathing and spit oscillation. However, the
4
5 521 morphodynamic impact of positive sea level anomalies during NAO negative winters
6
7 522 (Calafat et al., 2012) and how it may interact with longer term trends of SLR is an open
8
9
10 523 question. As is the impact of the complex wind-induced circulation (Salles et al., 2015)
11
12 524 on inlet morphodynamics. Nonetheless, these questions fall beyond the scope of the
13
14
15 525 present work.
16
17 526

19 527 **Synthesis**

20
21 528 Despite these latter questions, a combination of processes exists that may well have
22
23 529 contributed to the north-south oscillations of the spit-end observed on charts and aerial
24
25
26 530 photographs, between 1768 and 2014.

27
28 531 Variations in the wave climate associated with North Atlantic atmospheric state, very
29
30 532 likely modified sediment transport patterns near the spit-end; and trends in sea level
31
32 533 variations have modulated inlet dimensions, ultimately forcing the spit-end to retreat
33
34
35 534 when the inlet enlarged faster than it was migrating and allowing the spit-end to advance
36
37
38 535 otherwise. These two drivers make it possible to explain the spit decays and growths
39
40 536 over the entire study period and at the temporal scale resolved by that cartographic
41
42 537 data. Identifying a dominant mechanism is tricky though.

43
44 538 On the one hand, since the turn of the 20th century, the spit has then been able to
45
46
47 539 durably grow when the rate of SLR was moderate, as between 1930 and 1970.

48
49 540 Otherwise, when sea level has risen faster, like before 1930 or since 1970, the spit-end
50
51 541 has been unstable or has retreated. This indicates the existence of an upper limit to the
52
53
54 542 rate of SLR (around 2 mm.y⁻¹ according data in Table 2), above which spit growth is

1
2
3 543 annihilated. On the other hand, even though regional SLR remained moderate until the
4
5 544 late 1970s, the intensification of the alongshore wave power alone have trigger the spit
6
7 545 retreat in the early 1970s. The next step would then be to implement a numerical
8
9 546 morphodynamic model to rigorously evaluate the respective and relative contribution of
10
11 547 both forcing.
12
13
14 548 Finally, independently from the existence of a dominant mechanism, the exceptional
15
16 549 evolution during the first half of the 19th century was certainly produced by in-phase
17
18 550 destructive and constructive forces: from the spit point of view, it must have resulted
19
20 551 from synchronous constructive forces, exacerbated by the Dalton Minimum, followed by
21
22 552 synchronous destructive forces. This certainly agrees with the duality of wave climate
23
24 553 and sea level relations in terms of geomorphological impacts. However, it does not
25
26 554 answer the question of the interplay between these two drivers.
27
28
29
30
31
32

33 556 **Conclusions**

34
35
36 557 Detailed observations of the Cap Ferret spit-end over the last 250 years reveal
37
38 558 geomorphological changes of a remarkable magnitude. Owing to the temporal
39
40 559 coverage, it seems possible to explain the apparent cyclical nature of this dynamic by a
41
42 560 combination of climatic shifts and sea-level variations, although without considering an
43
44 561 eventual relationship between these two drivers.
45
46
47 562 First, all documented phases of spit growth were found during periods dominated by the
48
49 563 negative phase of the North Atlantic Oscillation in winter. Inversely, the spit has
50
51 564 retreated when the NAO shifted towards a positive-phase dominance. The relationship
52
53 565 between NAO and local wave climate make the wave climate a good candidate to
54
55
56
57
58
59
60

1
2
3 566 explain this behaviour. During the positive phase of the NAO, higher ocean waves
4
5 567 and/or clockwise shifts of the waves' mean direction accelerate alongshore sediment
6
7 568 transport (LST), which, counter intuitively and like it has been observed and modelled
8
9
10 569 elsewhere, contribute the updrift erosion of the spit-end.
11
12 570 In the second place, spit-end retreats and instabilities were also in phase with periods of
13
14 571 rapid or accelerating sea-level rise SLR. Synchronous expansions of the adjacent inlet
15
16 572 pointed at the impact of SLR on tidal prism. Indeed, enhanced tidal prism under
17
18 573 accelerating SLR may well exacerbate the ongoing adaptation of the whole Bay of
19
20 574 Arcachon to secular SLR, ultimately forcing the spit-end to retreat when the inlet
21
22 575 enlarges faster than it migrates downdrift.
23
24
25
26 576 Locally, these findings advocate a dominance of allocyclic mechanisms over the
27
28 577 autocyclic behaviour proposed by Michel and Howa (1997). Somehow this goes along
29
30 578 with the results of Allard et al. (2008) and Poirier et al. (2017), although the opposed
31
32 579 behaviour of Cap Ferret and Arçay spits regarding wave climate suggest that coastal
33
34 580 barrier spits response to increased LST may differ regarding if SLR is or not turning
35
36 581 spits' adjacent shoals into sediment sinks.
37
38
39 582 In a broader perspective, the present results further highlight the vulnerability to SLR of
40
41 583 barrier-spit backed by large estuaries. Given this, they may also serve to detect coastal
42
43 584 adjustments driven by climate change.
44
45
46
47 585

586 **Acknowledgments**

587 A.N. was funded under a BRGM PhD grant with the support of the *Région Aquitaine*
588 council and the *Syndicat Intercommunal du Bassin d'Arcachon*. We kindly acknowledge

1
2
3 589 Xavier Bertin (*CNRS-Université de La Rochelle*), for providing us with the wave
4
5 590 hindcast, as well as our office colleagues Anais Hoareau and Anne Fondin for digitizing
6
7 591 the bathymetric charts before 2001. We are grateful to our colleagues Thomas Bulteau,
8
9 592 Bruno Castelle and Gonéri Le Cozannet, and to Giovanni Coco from the University of
10
11 593 Auckland for their constructive feedback on an earlier version of the manuscript. We
12
13 594 also thank Jennifer Simeon from Pessac based GEOSAT for proof reading the
14
15 595 manuscript's final version. The geomorphological data can be requested by contacting
16
17 596 the first author or the *Observatoire de la Côte Aquitaine* ([http://www.observatoire-cote-](http://www.observatoire-cote-aquitaine.fr/)
18
19 597 [aquitaine.fr/](http://www.observatoire-cote-aquitaine.fr/)).
20
21
22
23
24 598

599 **References**

- 25
26
27
28
29 600 Aagaard T, Nielsen J, Jensen SG, Friderichsen J. 2004. Longshore sediment transport and coastal erosion at
30 601 Skallingen, Denmark. *Geografisk Tidsskrift-Danish Journal of Geography* **104** : 5–14. DOI:
31 602 10.1080/00167223.2004.10649499
- 32
33 603 Aagaard T, Sørensen P. 2013. Sea level rise and the sediment budget of an eroding barrier on the Danish North Sea
34 604 coast. *Journal of Coastal Research* **65** : 434–439. DOI: 10.2112/SI65-074.1
- 35
36 605 Allard J, Bertin X, Chaumillon E, Pouget F. 2008. Sand spit rhythmic development: A potential record of wave
37 606 climate variations? Arçay Spit, western coast of France. *Marine Geology* **253** : 107–131. DOI:
38 607 10.1016/j.margeo.2008.05.009
- 39
40 608 Allard J, Chaumillon E, Féliès H. 2009. A synthesis of morphological evolutions and Holocene stratigraphy of a
41 609 wave-dominated estuary: The Arcachon lagoon, SW France. *Continental Shelf Research* **29** : 957–969. DOI:
42 610 10.1016/j.csr.2008.11.017
- 43
44 611 Ashton AD, Nienhuis J, Ells K. 2016. On a neck, on a spit: controls on the shape of free spits. *Earth Surface*
45 612 *Dynamics* **4** : 193–210. DOI: 10.5194/esurf-4-193-2016
- 46
47 613 Aubié S, Tastet J-P. 2000. Coastal Erosion, Processes and Rates: An Historical Study of the Gironde Coastline,
48 614 Southwestern France. *Journal of Coastal Research* **16** : 756–767.
- 49
50 615 Barnard PL, Allan J, Hansen JE, Kaminsky GM, Ruggiero P, Doria A. 2011. The impact of the 2009-10 El Niño
51 616 Modoki on U.S. West Coast beaches. *Geophysical Research Letters* **38** : n/a-n/a. DOI: 10.1029/2011GL047707
- 52
53 617 Barnston AG, Livezey RE. 1987. Classification, Seasonality and Persistence of Low-Frequency Atmospheric
54 618 Circulation Patterns. *Monthly Weather Review* **115** : 1083–1126. DOI: 10.1175/1520-
55 619 0493(1987)115<1083:CSAPOL>2.0.CO;2

- 1
2
3 620 Bertin X, Fortunato AB, Oliveira A. 2009. A modeling-based analysis of processes driving wave-dominated inlets.
4 621 Continental Shelf Research **29** : 819–834. DOI: 10.1016/j.csr.2008.12.019
5
- 6 622 Bertin X, Li K, Roland A, Bidlot J-R. 2015. The contribution of short-waves in storm surges: Two case studies in
7 623 the Bay of Biscay. Continental Shelf Research **96** : 1–15. DOI: 10.1016/j.csr.2015.01.005
8
- 9 624 Bruneau N, Fortunato AB, Dodet G, Freire P, Oliveira A, Bertin X. 2011. Future evolution of a tidal inlet due to
10 625 changes in wave climate, Sea level and lagoon morphology (Óbidos lagoon, Portugal). Continental Shelf Research
11 626 **31** : 1915–1930. DOI: 10.1016/j.csr.2011.09.001
12
- 13 627 Bruun P. 1978. Stability of Coastal Inlets: Theory and Engineering . Elsevier. [online] Available from:
14 628 <http://www.sciencedirect.com/science/bookseries/01651250/23>
15
- 16 629 Calafat FM, Chambers DP, Tsimplis MN. 2012. Mechanisms of decadal sea level variability in the eastern North
17 630 Atlantic and the Mediterranean Sea. Journal of Geophysical Research: Oceans **117** : n/a-n/a. DOI:
18 631 10.1029/2012JC008285
19
- 20 632 Caspari E. 1872. Rapport sur l'exploration des Passes du Bassin d'Arcachon
21
- 22 633 Castelle B, Guillot B, Marieu V, Chaumillon E, Hanquiez V, Bujan S, Poppeschi C. 2018. Spatial and temporal
23 634 patterns of shoreline change of a 280-km high-energy disrupted sandy coast from 1950 to 2014: SW France.
24 635 Estuarine, Coastal and Shelf Science **200** : 212–223. DOI: 10.1016/j.ecss.2017.11.005
25
- 26 636 Cayocca F. 2001. Long-term morphological modeling of a tidal inlet: the Arcachon Basin, France. Coastal
27 637 Engineering **42** : 115–142. DOI: 10.1016/S0378-3839(00)00053-3
28
- 29 638 Cazenave A, Le Cozannet G. 2014. Sea level rise and its coastal impacts. Earth's Future **2** : 15–34. DOI:
30 639 10.1002/2013EF000188
31
- 32 640 CETMEF. n.d. CANDHIS (03302) - Bouée Cap Ferret [online] Available from:
33 641 [http://candhis.cetmef.developpement-](http://candhis.cetmef.developpement-durable.gouv.fr/campagne/?idcampagne=b6d767d2f8ed5d21a44b0e5886680cb9)
34 642 [durable.gouv.fr/campagne/?idcampagne=b6d767d2f8ed5d21a44b0e5886680cb9](http://candhis.cetmef.developpement-durable.gouv.fr/campagne/?idcampagne=b6d767d2f8ed5d21a44b0e5886680cb9) (Accessed 6 March 2017)
35
- 36 643 Charles E, Idier D, Thiébot J, Le Cozannet G, Pedreros R, Arduin F, Planton S. 2012. Present Wave Climate in the
37 644 Bay of Biscay: Spatiotemporal Variability and Trends from 1958 to 2001. Journal of Climate **25** : 2020–2039. DOI:
38 645 10.1175/JCLI-D-11-00086.1
39
- 40 646 Chowdhury P, Behera MR. 2017. Effect of long-term wave climate variability on longshore sediment transport
41 647 along regional coastlines. Progress in Oceanography **156** : 145–153. DOI: 10.1016/j.pocean.2017.06.001
42
- 43 648 Clarke M, Rendell H, Tastet J-P, Clavé B, Massé L. 2002. Late-Holocene sand invasion and North Atlantic
44 649 storminess along the Aquitaine Coast, southwest France. The Holocene **12** : 231–238. DOI:
45 650 10.1191/0959683602hl539rr
46
- 47 651 Clemmensen LB, Richardt N, Anderson C. 2001. Holocene sea-level variation and spit development: data from
48 652 Skagen Odde, Denmark. The Holocene **11** : 323–331. DOI: 10.1191/095968301667877044
49
- 50 653 Cook ER, D'Arrigo RD, Mann ME. 2002. A Well-Verified, Multiproxy Reconstruction of the Winter North Atlantic
51 654 Oscillation Index since a.d. 1400. Journal of Climate **15** : 1754–1764. DOI: 10.1175/1520-
52 655 0442(2002)015<1754:AWVMRO>2.0.CO;2
53
- 54 656 Davis RA. 2013. Evolution of Coastal Landforms. In Treatise on Geomorphology , . Elsevier; 417–448. [online]
55 657 Available from: <http://linkinghub.elsevier.com/retrieve/pii/B9780123747396002931> (Accessed 20 April 2016)
56
57
58
59
60

- 1
2
3 658 Dissanayake DMPK, Ranasinghe R, Roelvink JA. 2012. The morphological response of large tidal inlet/basin
4 659 systems to relative sea level rise. *Climatic Change* **113** : 253–276. DOI: 10.1007/s10584-012-0402-z
5
- 6 660 Dodet G, Bertin X, Taborda R. 2010. Wave climate variability in the North-East Atlantic Ocean over the last six
7 661 decades. *Ocean Modelling* **31** : 120–131. DOI: 10.1016/j.ocemod.2009.10.010
8
- 9 662 Féliens H, Faugères J-C. 1998. Facies and geometry of tidal channel-fill deposits (Arcachon Lagoon, SW France).
10 663 *Marine Geology* **150** : 131–148. DOI: 10.1016/S0025-3227(98)00049-8
11
- 12 664 Féliens H, Lericolais G. 2005. Internal architecture of an incised valley-fill on a wave- and tide-dominated coast (the
13 665 Leyre incised valley, Bay of Biscaye, France). *Comptes Rendus Geoscience* **337** : 1257–1266. DOI:
14 666 10.1016/j.crte.2005.06.005
15
- 16 667 Féliens H, Lericolais G, Posamentier HW. 2010. Comparison of wave- and tide-dominated incised valleys: specific
17 668 processes controlling systems tract architecture and reservoir geometry. *Bulletin de la Societe Geologique de France*
18 669 **181** : 171–181. DOI: 10.2113/gssgfbull.181.2.171
19
- 20 670 FitzGerald D, Georgiou I, Miner M. 2015. Estuaries and Tidal Inlets. In *Coastal Environments and Global Change* ,
21 671 Masselink G and Gehrels R (eds). John Wiley & Sons, Ltd: Chichester, UK; 268–298. [online] Available from:
22 672 <http://doi.wiley.com/10.1002/9781119117261.ch12> (Accessed 19 May 2016)
23
- 24 673 FitzGerald DM, Fenster MS, Argow BA, Buynevich IV. 2008. Coastal Impacts Due to Sea-Level Rise. *Annual*
25 674 *Review of Earth and Planetary Sciences* **36** : 601–647. DOI: 10.1146/annurev.earth.35.031306.140139
26
- 27 675 FitzGerald DM, Kraus NC, Hands EB. 2001. Natural mechanisms of sediment bypassing at tidal inlets . U.S. Army
28 676 Engineer Research and Development Center: Vicksburg, MS
29
- 30 677 Fortunato AB et al. 2014. Morphological evolution of an ephemeral tidal inlet from opening to closure: The
31 678 Albufeira inlet, Portugal. *Continental Shelf Research* **73** : 49–63. DOI: 10.1016/j.csr.2013.11.005
32
- 33 679 Fortunato AB, Oliveira A. 2005. Influence of Intertidal Flats on Tidal Asymmetry. *Journal of Coastal Research* **215** :
34 680 1062–1067. DOI: 10.2112/03-0089.1
35
- 36 681 Friedrichs CT, Aubrey DG. 1988. Non-linear tidal distortion in shallow well-mixed estuaries: a synthesis. *Estuarine,*
37 682 *Coastal and Shelf Science* **27** : 521–545. DOI: 10.1016/0272-7714(88)90082-0
38
- 39 683 Fruergaard M, Andersen TJ, Johannessen PN, Nielsen LH, Pejrup M. 2013. Major coastal impact induced by a
40 684 1000-year storm event. *Scientific Reports* **3** DOI: 10.1038/srep01051 [online] Available from:
41 685 <http://www.nature.com/articles/srep01051> (Accessed 11 April 2016)
42
- 43 686 Fruergaard M, Andersen TJ, Nielsen LH, Johannessen PN, Aagaard T, Pejrup M. 2015. High-resolution
44 687 reconstruction of a coastal barrier system: impact of Holocene sea-level change. *Sedimentology* **62** : 928–969. DOI:
45 688 10.1111/sed.12167
46
- 47 689 Glueck MF, Stockton CW. 2001. Reconstruction of the North Atlantic Oscillation, 1429-1983. *International Journal*
48 690 *of Climatology* **21** : 1453–1465. DOI: 10.1002/joc.684
49
- 50 691 Hayes MO. 1979. Barrier island morphology as a function of tidal and wave regime. In *Barrier Islands, from the*
51 692 *Gulf of St. Lawrence to the Gulf of Mexico* , . Leatherman, S.; 1–27.
52
- 53 693 Hoan LX, Hanson H, Larson M, Kato S. 2011. A mathematical model of spit growth and barrier elongation:
54 694 Application to Fire Island Inlet (USA) and Badreveln Spit (Sweden). *Estuarine, Coastal and Shelf Science* **93** : 468–
55 695 477. DOI: 10.1016/j.ecss.2011.05.033
56
57
58
59
60

- 1
2
3 696 Holgate SJ, Matthews A, Woodworth PL, Rickards LJ, Tamisiea ME, Bradshaw E, Foden PR, Gordon KM,
4 697 Jevrejeva S, Pugh J. 2013. New Data Systems and Products at the Permanent Service for Mean Sea Level. *Journal of*
5 698 *Coastal Research* **288** : 493–504. DOI: 10.2112/JCOASTRES-D-12-00175.1
6
7 699 Hubbard DK, Oertel GF, Nummedal D. 1979. The Role of Waves and Tidal Currents in the Development of Tidal-
8 700 inlet Sedimentary Structures and Sand Body Geometry: Examples from North Carolina, South Carolina, and
9 701 Georgia. *SEPM Journal of Sedimentary Research* **Vol. 49** DOI: 10.1306/212F78B5-2B24-11D7-
10 702 8648000102C1865D [online] Available from: [http://jsedres.sepmonline.org/cgi/doi/10.1306/212F78B5-2B24-11D7-](http://jsedres.sepmonline.org/cgi/doi/10.1306/212F78B5-2B24-11D7-8648000102C1865D)
11 703 [8648000102C1865D](http://jsedres.sepmonline.org/cgi/doi/10.1306/212F78B5-2B24-11D7-8648000102C1865D) (Accessed 26 September 2016)
12
13 704 Hurrell JW. 1995. Decadal Trends in the North Atlantic Oscillation: Regional Temperatures and Precipitation.
14 705 *Science* **269** : 676–679. DOI: 10.1126/science.269.5224.676
15
16 706 Hurrell JW. 2015. The Climate Data Guide: Hurrell North Atlantic Oscillation (NAO) Index (Station-based) [online]
17 707 Available from: <https://climatedataguide.ucar.edu/climate-data/hurrell-north-atlantic-oscillation-nao-index-pc-based>
18 708 (Accessed 14 August 2015)
19
20 709 Hurrell JW. 2019. The Climate Data Guide: Hurrell North Atlantic Oscillation (NAO) Index (PC-based) [online]
21 710 Available from: <https://climatedataguide.ucar.edu/climate-data/hurrell-north-atlantic-oscillation-nao-index-pc-based>
22 711 (Accessed 26 January 2019)
23
24 712 Hurrell JW, Deser C. 2009. North Atlantic climate variability: The role of the North Atlantic Oscillation. *Journal of*
25 713 *Marine Systems* **78** : 28–41. DOI: 10.1016/j.jmarsys.2008.11.026
26
27 714 Idier D, Castelle B, Charles E, Mallet C. 2013. Longshore sediment flux hindcast: spatio-temporal variability along
28 715 the SW Atlantic coast of France. *Journal of Coastal Research* **165** : 1785–1790. DOI: 10.2112/SI65-302.1
29
30 716 Ineson S, Scaife AA, Knight JR, Manners JC, Dunstone NJ, Gray LJ, Haigh JD. 2011. Solar forcing of winter
31 717 climate variability in the Northern Hemisphere. *Nature Geoscience* **4** : 753–757. DOI: 10.1038/ngeo1282
32
33 718 Jarrett JT. 1976. Tidal Prism - Inlet Area Relationships . Army Engineer Waterways Experiment Station: Vicksburg
34 719 MS [online] Available from: http://cirp.usace.army.mil/pubs/archive/GITI-Report_Number_3.pdf
35
36 720 Jevrejeva S, Moore JC, Grinsted A, Matthews AP, Spada G. 2014. Trends and acceleration in global and regional
37 721 sea levels since 1807. *Global and Planetary Change* **113** : 11–22. DOI: 10.1016/j.gloplacha.2013.12.004
38
39 722 Jones PD, Jonsson T, Wheeler D. 1997. Extension to the North Atlantic oscillation using early instrumental pressure
40 723 observations from Gibraltar and south-west Iceland. *International Journal of Climatology* **17** : 1433–1450. DOI:
41 724 10.1002/(SICI)1097-0088(19971115)17:13<1433::AID-JOC203>3.0.CO;2-P
42
43 725 Kalnay E et al. 1996. The NCEP/NCAR 40-Year Reanalysis Project. *Bulletin of the American Meteorological*
44 726 *Society* **77** : 437–471. DOI: 10.1175/1520-0477(1996)077<0437:TNYRP>2.0.CO;2
45
46 727 Kirwan ML, Murray AB. 2008. Tidal marshes as disequilibrium landscapes? Lags between morphology and
47 728 Holocene sea level change. *Geophysical Research Letters* **35** DOI: 10.1029/2008GL036050 [online] Available from:
48 729 <http://doi.wiley.com/10.1029/2008GL036050> (Accessed 19 April 2016)
49
50 730 Kraus NC. 1998. Inlet Cross-Sectional Area Calculated by Process-Based Model. presented at the Conference on
51 731 Coastal Engineering. Copenhagen, Denmark. 3265–3278 pp. [online] Available from: [https://icce-ojs-](https://icce-ojs-tamu.tdl.org/icce/index.php/icce/article/view/5839)
52 732 [tamu.tdl.org/icce/index.php/icce/article/view/5839](https://icce-ojs-tamu.tdl.org/icce/index.php/icce/article/view/5839) (Accessed 28 September 2016)
53
54 733 Kraus NC. 2000. Reservoir Model of Ebb-Tidal Shoal Evolution and Sand Bypassing. *Journal of Waterway, Port,*
55 734 *Coastal, and Ocean Engineering* **126** : 305–313. DOI: 10.1061/(ASCE)0733-950X(2000)126:6(305)
56
57
58
59
60

- 1
2
3 735 Kraus NC, Seabergh WC. 2002. Inlet spits and maintenance of navigation channels . U.S. Army Engineer Research
4 736 and Development Center: Vicksburg, MS [online] Available from:
5 737 <http://acwc.sdp.sirsi.net/client/search/asset/1000403> (Accessed 13 June 2016)
6
7 738 Lapeyre. 1925. Cartes du Pays de Buch, 1318 à 1913
8
9 739 Larson M, Kraus NC, Connell KJ. 2007. MODELING SEDIMENT STORAGE AND TRANSFER FOR
10 740 SIMULATING REGIONAL COASTAL EVOLUTION. presented at the Proceedings of the 30th International
11 741 Conference. San Diego, California, USA. 3924–3936 pp. April [online] Available from:
12 742 http://www.worldscientific.com/doi/abs/10.1142/9789812709554_0330 (Accessed 22 March 2019)
13
14 743 Luterbacher J et al. 2001. Extending North Atlantic oscillation reconstructions back to 1500. Atmospheric Science
15 744 Letters **2** : 114–124. DOI: 10.1006/asle.2002.0047
16
17 745 Luterbacher J, Schmutz C, Gyalistras D, Xoplaki E, Wanner H. 1999. Reconstruction of monthly NAO and EU
18 746 indices back to AD 1675. Geophysical Research Letters **26** : 2745–2748. DOI: 10.1029/1999GL900576
19
20 747 van Maanen B, Coco G, Bryan KR, Friedrichs CT. 2013. Modeling the morphodynamic response of tidal
21 748 embayments to sea-level rise. Ocean Dynamics **63** : 1249–1262. DOI: 10.1007/s10236-013-0649-6
22
23 749 Masselink G, Austin M, Scott T, Poate T, Russell P. 2014. Role of wave forcing, storms and NAO in outer bar
24 750 dynamics on a high-energy, macro-tidal beach. Geomorphology **226** : 76–93. DOI: 10.1016/j.geomorph.2014.07.025
25
26 751 Masselink G, Castelle B, Scott T, Dodet G, Suarez S, Jackson D, Floc'h F. 2016. Extreme wave activity during
27 752 2013/2014 winter and morphological impacts along the Atlantic coast of Europe. Geophysical Research Letters **43** :
28 753 2135–2143. DOI: 10.1002/2015GL067492
29
30 754 Mazzarella A, Scafetta N. 2012. Evidences for a quasi 60-year North Atlantic Oscillation since 1700 and its
31 755 meaning for global climate change. Theoretical and Applied Climatology **107** : 599–609. DOI: 10.1007/s00704-011-
32 756 0499-4
33
34 757 Michel D, Howa HL. 1997. Morphodynamic behaviour of a tidal inlet system in a mixed-energy environment.
35 758 Physics and Chemistry of the Earth **22** : 339–343. DOI: 10.1016/S0079-1946(97)00155-9
36
37 759 Nahon A. 2018. Ongoing morphological evolution of a Holocene coastal barrier-spit - The Cap Ferret, bounded by
38 760 the Bay of Arcachon tidal inlet, PhD Thesis, University of Bordeaux: Bordeaux, France, October
39
40 761 Nahon A, Bertin X, Fortunato AB, Oliveira A. 2012. Process-based 2DH morphodynamic modeling of tidal inlets:
41 762 A comparison with empirical classifications and theories. Marine Geology **291–294** : 1–11. DOI:
42 763 10.1016/j.margeo.2011.10.001
43
44 764 Nahon A, Idier D, Fenies H, Mugica J, Senechal N, Mallet C. 2015. Role of north atlantic climate variability on
45 765 barrier-spit oscillations: the Cap Ferret. presented at the Coastal Sediments 2015. San Diego. July [online] Available
46 766 from: http://www.worldscientific.com/doi/abs/10.1142/9789814689977_0240 (Accessed 21 April 2016)
47
48 767 Newton A et al. 2014. An overview of ecological status, vulnerability and future perspectives of European large
49 768 shallow, semi-enclosed coastal systems, lagoons and transitional waters. Estuarine, Coastal and Shelf Science **140** :
50 769 95–122. DOI: 10.1016/j.ecss.2013.05.023
51
52 770 Nichols M, Allen G. 1981. Sedimentary processes in coastal lagoons. Unesco Technical Papers In Marine Science :
53 771 27–80.
54
55 772 O'Brien MP. 1931. Estuary tidal prisms related to entrance areas. Civil Engineering **1** : 738–739.
56
57
58
59
60

- 1
2
3 773 Ortega P, Lehner F, Swingedouw D, Masson-Delmotte V, Raible CC, Casado M, Yiou P. 2015. A model-tested
4 774 North Atlantic Oscillation reconstruction for the past millennium. *Nature* **523** : 71–74.
5
6 775 PAB. 1985. Etude de l'évolution du littoral de la presqu'île du Cap Ferret . Port Autonome de Bordeaux, Direction
7 776 de l'aménagement et de l'environnement maritimes: Bordeaux, France
8
9 777 Plus M, Dumas F, Stanisière J-Y, Maurer D. 2009. Hydrodynamic characterization of the Arcachon Bay, using
10 778 model-derived descriptors. *Continental Shelf Research* **29** : 1008–1013. DOI: 10.1016/j.csr.2008.12.016
11
12 779 Poirier C, Tessier B, Chaumillon É, Bertin X, Fruergaard M, Mouzéd D, Noël S, Weill P, Wöppelmann G. 2017.
13 780 Decadal changes in North Atlantic atmospheric circulation patterns recorded by sand spits since 1800CE.
14 781 *Geomorphology* **281** : 1–12. DOI: 10.1016/j.geomorph.2016.12.028
15
16 782 Ranasinghe R, Duong TM, Uhlenbrook S, Roelvink D, Stive M. 2012. Climate-change impact assessment for inlet-
17 783 interrupted coastlines. *Nature Climate Change* **3** : 83–87. DOI: 10.1038/nclimate1664
18
19 784 Ridderinkhof W, Hoekstra P, van der Vegt M, de Swart HE. 2016. Cyclic behavior of sandy shoals on the ebb-tidal
20 785 deltas of the Wadden Sea. *Continental Shelf Research* **115** : 14–26. DOI: 10.1016/j.csr.2015.12.014
21
22 786 Roland A, Zhang YJ, Wang HV, Meng Y, Teng Y-C, Maderich V, Brovchenko I, Dutour-Sikiric M, Zanke U. 2012.
23 787 A fully coupled 3D wave-current interaction model on unstructured grids. *Journal of Geophysical Research: Oceans*
24 788 **117** : n/a-n/a. DOI: 10.1029/2012JC007952
25
26 789 Salles P, Valle-Levinson A, Sottolichio A, Senechal N. 2015. Wind-driven modifications to the residual circulation
27 790 in an ebb-tidal delta: Arcachon Lagoon, Southwestern France. *Journal of Geophysical Research: Oceans* **120** : 728–
28 791 740. DOI: 10.1002/2014JC010311
29
30 792 van der Schrier G, Barkmeijer J. 2005. Bjerknes' hypothesis on the coldness during AD 1790–1820 revisited.
31 793 *Climate Dynamics* **25** : 537–553. DOI: 10.1007/s00382-005-0053-0
32
33 794 Semedo A, Weisse R, Behrens A, Sterl A, Bengtsson L, Günther H. 2013. Projection of Global Wave Climate
34 795 Change toward the End of the Twenty-First Century. *Journal of Climate* **26** : 8269–8288. DOI: 10.1175/JCLI-D-12-
35 796 00658.1
36
37 797 Senechal N, Sottolichio A, Bertrand F, Goeldner-Gianella L, Garlan T. 2013. Observations of waves' impact on
38 798 currents in a mixed-energy tidal inlet: Arcachon on the southern French Atlantic coast. *Journal of Coastal Research*
39 799 **165** : 2053–2058. DOI: 10.2112/S165-347.1
40
41 800 Shindell DT. 2001. Solar Forcing of Regional Climate Change During the Maunder Minimum. *Science* **294** : 2149–
42 801 2152. DOI: 10.1126/science.1064363
43
44 802 Splinter KD, Davidson MA, Golshani A, Tomlinson R. 2012. Climate controls on longshore sediment transport.
45 803 *Continental Shelf Research* **48** : 146–156. DOI: 10.1016/j.csr.2012.07.018
46
47 804 Svendsen IA. 2006. Linear Waves. In *Introduction to Nearshore Hydrodynamics* , . World Scientific; 49–205.
48 805 [online] Available from: <https://books.google.fr/books?id=g7-PHmrvQcC>
49
50 806 Walton, Jr. TL, Adams WD. 1976. Capacity of inlet outer bars to store sand. In *Proceedings of the 15th Coastal*
51 807 *Engineering Conference, Honolulu, HI* , . ASCE; 1919–1937. [online] Available from: [https://icce-ojs-](https://icce-ojs-tamu.tdl.org/icce/index.php/icce/article/viewFile/3161/2825)
52 808 [tamu.tdl.org/icce/index.php/icce/article/viewFile/3161/2825](https://icce/index.php/icce/article/viewFile/3161/2825)
53
54 809 van der Wegen M. 2013. Numerical modeling of the impact of sea level rise on tidal basin morphodynamics. *Journal*
55 810 *of Geophysical Research: Earth Surface* **118** : 447–460. DOI: 10.1002/jgrf.20034
56
57
58
59
60

- 1
2
3 811 Wiggins M, Scott T, Masselink G, Russell P, Castelle B, Dodet G. 2017. THE ROLE OF MULTI-DECADAL
4 812 CLIMATE VARIABILITY IN CONTROLLING COASTAL DYNAMICS: RE-INTERPRETATION OF THE
5 813 ‘LOST VILLAGE OF HALLSANDS’’.’ Helsingor, Denmark. June [online] Available from: [https://hal.archives-](https://hal.archives-ouvertes.fr/hal-01578356)
6 814 [ouvertes.fr/hal-01578356](https://hal.archives-ouvertes.fr/hal-01578356)
7
8 815 Wong PP, Losada IJ, Gattuso J-P, Hinkel J, Khattabi A, McInnes KL, Saito Y, Sallenger A. 2014. Coastal systems
9 816 and low-lying areas. In *Climate Change 2014: Impacts, Adaptation, and Vulnerability. Part A: Global and Sectoral*
10 817 *Aspects. Contribution of Working Group II to the Fifth Assessment Report of the Intergovernmental Panel of*
11 818 *Climate Change*, Field, C.B. et al. (eds). Cambridge, United Kingdom and New York, NY, USA; 361–409.
12
13 819 Wöppelmann G, Pouvreau N, Coulomb A, Simon B, Woodworth PL. 2008. Tide gauge datum continuity at Brest
14 820 since 1711: France’s longest sea-level record. *Geophysical Research Letters* **35** DOI: 10.1029/2008GL035783
15 821 [online] Available from: <http://doi.wiley.com/10.1029/2008GL035783> (Accessed 2 June 2016)
16
17 822 Zhou Z, Coco G, Jiménez M, Olabarrieta M, van der Wegen M, Townend I. 2014. Morphodynamics of river-
18 823 influenced back-barrier tidal basins: The role of landscape and hydrodynamic settings. *Water Resources Research* **50**
19 824 : 9514–9535. DOI: 10.1002/2014WR015891
20
21 825
22
23 826
24
25
26
27
28
29
30
31
32
33
34
35
36
37
38
39
40
41
42
43
44
45
46
47
48
49
50
51
52
53
54
55
56
57
58
59
60

827 **Tables**828 **Table 1.** Morphological parameters of the inlet throat between 1949 and 2014.

year	Channel volume (Mm ³)	Shoal volume (Mm ³)	Mean elevation (m NGF)	Morphological amplitude (Mm ³)
1949	32.14	59.48	-5.50	42.69
1969	30.02	54.20	-5.61	38.80
1979	30.02	43.21	-6.17	34.74
2001	33.93	61.41	-5.53	44.02
2014	38.62	60.58	-5.82	46.65
mean	32.53	55.78	-5.77	41.38

830 **Table 2.** Trends in Brest tidal gauge annual sea level data.

Periods	Linear trend, mm.y ⁻¹	Spit behaviour
1807-1835	-1.08	extending
1826-1872	0.14	retreating
1865-1909	-0.33	extending
1900-1934	2.5	retreating
1932-1972	1.26	extending
1968-2015	2.42	retreating

831

For Peer Review

832 **Table 3.** Comparison of hindcasted wave parameters and wave buoy observations.

Wave Field	BIAS (% of mean)	ERMS (% of mean)	Pearson Corr. coeff.
<i>Hs</i>	-1.16	43 cm	0.93
<i>WP</i>	-2.4	-	0.93
<i>wDir</i>	3.75° (0°)	-	-
<i>WPx</i>	-3.4 (1.7)	-	0.93 (0.93)
<i>WPy</i>	27.1 (1.7)	-	0.80 (0.81)

833

For Peer Review

1
2
3 834 **Figures**
4
5

6 835
7
8 836 **Figure 1** – Location maps. **a**) Bathymetry of the Bay of Biscay, bordering the
9
10 837 SW coast of France; **b**) Gironde sandy coast, between the Gironde Estuary and
11
12 838 the Bay of Arcachon, former estuary of the Leyre river and now a lagoon, semi-enclosed
13
14 839 by the Cap Ferret sand spit (coordinates given in Lambert 93, in meters); **c**)
15
16 840 Satellite Landsat 8 image of the Bay's tidal inlet in October 2014, showing the main
17
18 841 geomorphological units and the red dotted line indicating the 2014 coastline of the Cap
19
20 842 Ferret spit-end, on the inlet's updrift margin.
21
22
23
24
25

26 844 **Figure 2** – Nautical charts. **a**) Ordnance survey map from 1888, black circled
27
28 845 dots indicate control points used for georeferencing the map, red dashed line is the
29
30 846 coastline measured by GPS on 2014 spring, red stars indicate the 3 reference locations
31
32 847 used for georeferencing nautical charts; **b-e**) examples of nautical charts used
33
34 848 to measure the spit-end positions, indicated by asterisk symbols for every given date;
35
36 849 **f-g**) Satellite Landsat image of the Bay of Arcachon and its tidal inlet in October
37
38 850 2014.
39
40
41
42
43
44

45 852 **Figure 3** – Measuring the spit's extension relative to the position of Cap Ferret's
46
47 853 lighthouse. **Upper panels**: charts and coastlines from 1768 and 1826 and
48
49 854 Satellite Landsat 8 image from October 2014, red dotted lines represent the 2014
50
51 855 coastline and the red stars indicate the lighthouse's position, white dashed lines
52
53 856 materialize the axe onto which spit-end positions were orthogonally projected and
54
55
56
57
58
59
60

1
2
3 857 measured, the black sector in the right panel represents the spit-end migration range;
4
5 858 **lower panel**: the grey curve shows the spit-end path between 1768 and 1936,
6
7 859 grey error bars stand for historical charts and the black ones for modern charts, asterisk
8
9
10 860 symbol stand for spit-end positions in Figure 2**b-e**.

11
12 861
13
14 862 **Figure 4** – Positions of the Cap Ferret spit-end measured on aerial photographs.

15
16
17 863 **Upper panels**: series of aerial photographs of the spit-end, red dotted lines
18
19 864 represent the 2014 coastline, black asterisk symbols materialize the spit-end positions
20
21 865 for the given years, superimposed on photographs from 1934 and 1946 are the
22
23 866 shorelines reproduced from charts of 1932 and 1936 respectively; **lower panel**:
24
25 867 distance of the spit-end to lighthouse's position, black asterisk symbols correspond to
26
27 868 those on the upper panel.
28
29
30
31 869

32
33 870 **Figure 5** – Inlet throat bathymetric data. **a**) summer 2014 along transect
34
35 871 soundings; **b**) interpolated bathymetry with the -7 m NGF contours (black lines);
36
37 872 **c**) -7 m NGF contours superimposed onto October 2014 Landsat image;
38
39 873 **d**) erosion (blue) – deposition (red) patterns over the 12.74 km² area covered
40
41 874 by all 5 surveys between 1949 and 2014; **e-h**) channel volume (below -7 m
42
43 875 NGF) , shoal volume (above -7 m NGF), overlapping area mean depth (m NGF) and
44
45 876 inlet morphological amplitude over panel **d**'s area (**e**, **f** and
46
47 877 **h** are in percent of averaged values for all 5 surveys).
48
49
50
51 878

1
2
3 879 **Figure 6** – Brest tidal gauge Mean Sea Level (MSL) variation. **Upper panel**:
4
5 880 annual MSL data from 1807 to 2015 recovered from the PMSL observatory (Holgate et
6
7 881 al., 2013), black lines are the 11-year centred running mean of annual measurements
8
9 882 and the thick dotted red line is the quadratic fit of all the data; **lower panel**:
10
11 883 same as above with data from 20th century onward fitted with a 5th order polynomial
12
13 884 function.
14
15
16
17
18

19 886 **Figure 7** – Local, 54 m water depth wave hindcast. **Upper panel**: 90-day
20
21 887 running mean of the wave power (WP; linear wave theory approximation) 15 km
22
23 888 offshore Cap Ferret, solid blue line are wind wave model (WWM-II, Roland et al., 2012)
24
25 889 results with Bertin et al. (2015) setup, dotted black line are the wave buoy observations
26
27 890 (CETMEF, n.d.) between April 2011 and May 2014, data is normalized using mean WP
28
29 891 value over the hindcast period (1948-2014); **lower panel**: same as above with
30
31 892 the alongshore component of the wave power (WP_y); *r* values are
32
33 893 Pearson's linear correlation coefficients between plotted curves.
34
35
36
37
38
39

40 895 **Figure 8** – Spit-end path and cumulated winter NAO indices between 1768 and 2014.
41
42 896 **Upper panel**: the grey curve shows the distance from the spit-end to the Cap
43
44 897 Ferret lighthouse as on Figures 3&4 (red dotted frame is for next Figure 8's zoom);
45
46 898 **mid panel**: darker blue curve is the cumulated winter (DJFM) index of the NAO
47
48 899 reconstruction of Luterbacher et al. (1999), lighter blue curve is the same but for
49
50 900 (Hurrell's (2015) station-based (DJFM) index; **lower panel**: darker blue curve is
51
52 901 the cumulated winter (DJF) index of the NAO reconstruction of Ortega et al. (2015),
53
54
55
56
57
58
59
60

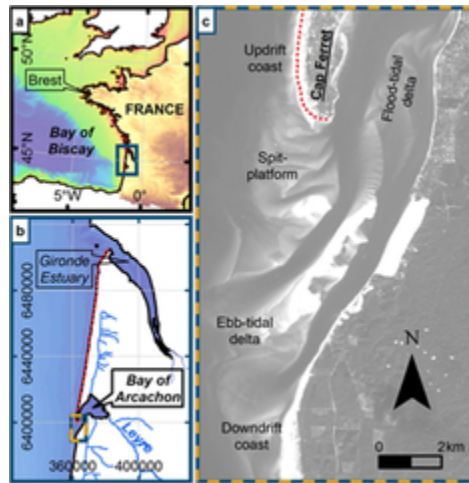
1
2
3 902 lighter blue curve is the same but for Hurrell's (2015) station-based (DJFM) index; on all
4
5 903 panels, orange shades indicate periods of spit elongation with the Dalton Minimum
6
7 904 period in darker orange, r values are Pearson's linear correlation
8
9
10 905 coefficients between plotted curves.

11
12 906
13 **Figure 9** – Evolution of the spit-inlet system across the Dalton Minimum (1780 – 1830).
14
15
16 908 Navigation charts from years 1768, 1813, 1826 and 1865; blue asterisks indicate the
17
18 909 positions of the spit terminus at the respective dates; black arrows materialize the inlet
19
20 910 minimal width; red and blue arrows materialize the position of respectively the northern
21
22 911 and southern channels; the dotted black line depicts the migration of the main inlet
23
24 912 shoal barycentre; common red stars, dotted white axis and dotted red line are the same
25
26
27 913 as in Figures 2 and 3.

28
29
30 914
31
32 915 **Figure 10** – NAO relationships with Cap Ferret's spit-end and local wave climate.
33
34 916 **Upper panel**: in grey is the path of the spit-end, as the distance from the spit-
35
36 917 end to the Cap Ferret lighthouse, as on Figures 3&4 and over since 1909,
37
38 918 superimposed blue curve is Hurrell's (2015) station-based NAO winter index, averaged
39
40 919 of 10 years preceding each observation; **lower panel**: same winter NAO index
41
42 920 curve as above, along with hindcasted alongshore winter wave power (WPy), averaged
43
44 921 in same fashion as the NAO index and normalized using mean WPy value over the
45
46 922 hindcast period (1948-2014); on both panels, orange shades indicate periods of spit
47
48 923 elongation, r values are Pearson's linear correlation coefficients between
49
50
51 924 plotted curves

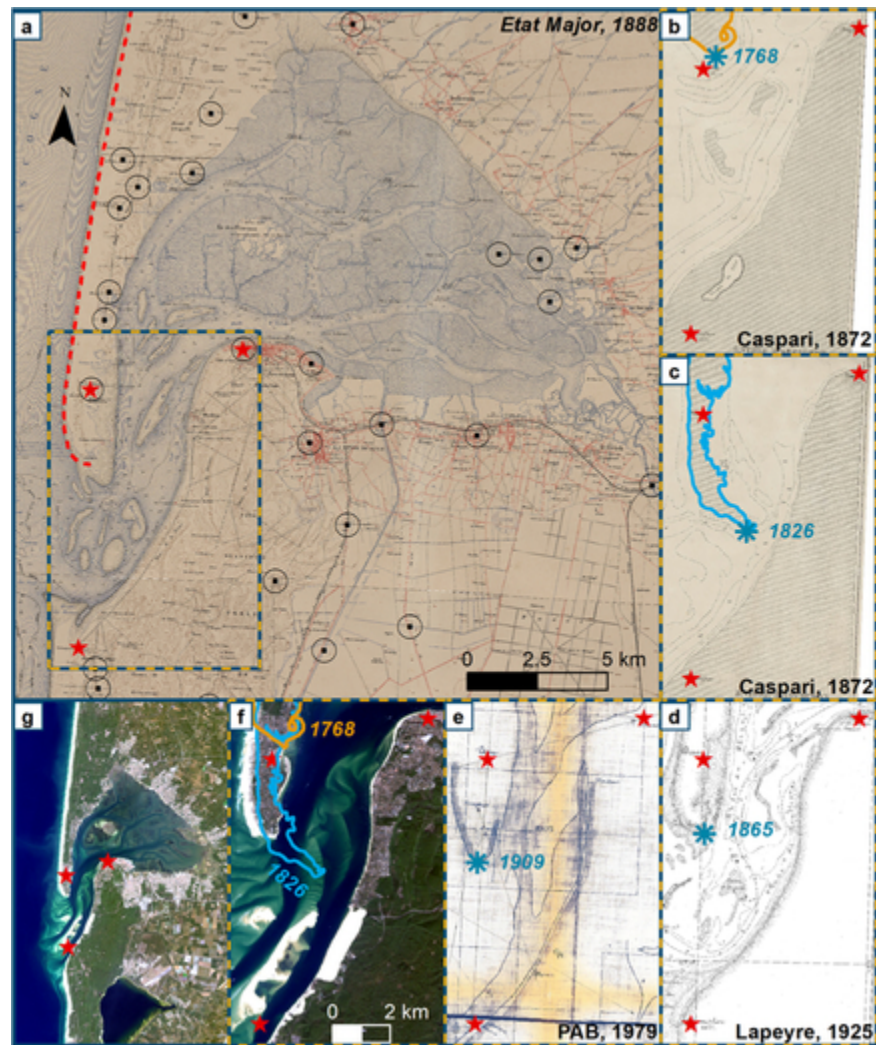
52
53
54
55 925

1
2
3 926 **Figure 11** – Sandspit’s morphological response to changes in mean wave direction.
4
5
6 927 **a**) spit-end response to a decrease of the averaged wave angle of incidence,
7
8 928 modelled by (and reproduced from) Ashton et al. (2016), dashed line represents initial
9
10 929 shoreline and shaded area represents the spit-end contours after waves became more
11
12 930 shore normal; **b**) same as panel **a**), but for an increase of the averaged
13
14 931 wave angle of incidence, or after waves became more oblique; **c**) dashed line
15
16 932 represents Cap Ferret spit-end in 1826, at the end of the Dalton Minimum, and shaded
17
18
19 933 area represents the spit-end in 1865.
20
21
22
23
24
25
26
27
28
29
30
31
32
33
34
35
36
37
38
39
40
41
42
43
44
45
46
47
48
49
50
51
52
53
54
55
56
57
58
59
60



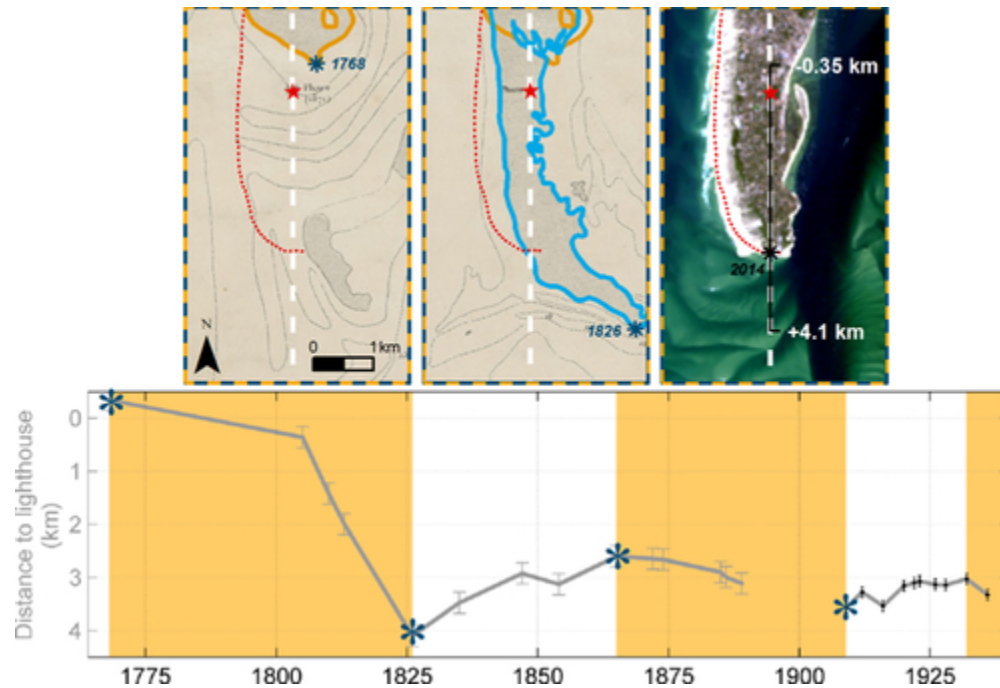
Location maps. **a)** Bathymetry of the Bay of Biscay, bordering the SW coast of France; **b)** Gironde sandy coast, between the Gironde Estuary and the Bay of Arcachon, former estuary of the Leyre river and now a lagoon, semi-enclosed by the Cap Ferret sand spit (coordinates given in Lambert 93, in meters); **c)** Satellite Landsat 8 image of the Bay's tidal inlet in October 2014, showing the main geomorphological units and the red dotted line indicating the 2014 coastline of the Cap Ferret spit-end, on the inlet's updrift margin.

19x20mm (300 x 300 DPI)



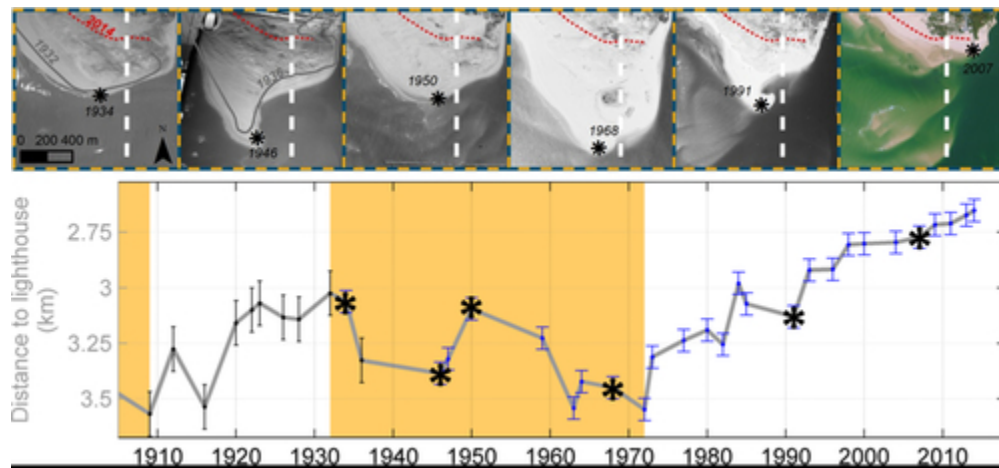
Nautical charts. **a)** Ordnance survey map from 1888, black circled dots indicate control points used for georeferencing the map, red dashed line is the coastline measured by GPS on 2014 spring, red stars indicate the 3 reference locations used for georeferencing nautical charts; **b-e)** examples of nautical charts used to measure the spit-end positions, indicated by asterisk symbols for every given date; **f-g)** Satellite Landsat image of the Bay of Arcachon and its tidal inlet in October 2014.

36x44mm (300 x 300 DPI)



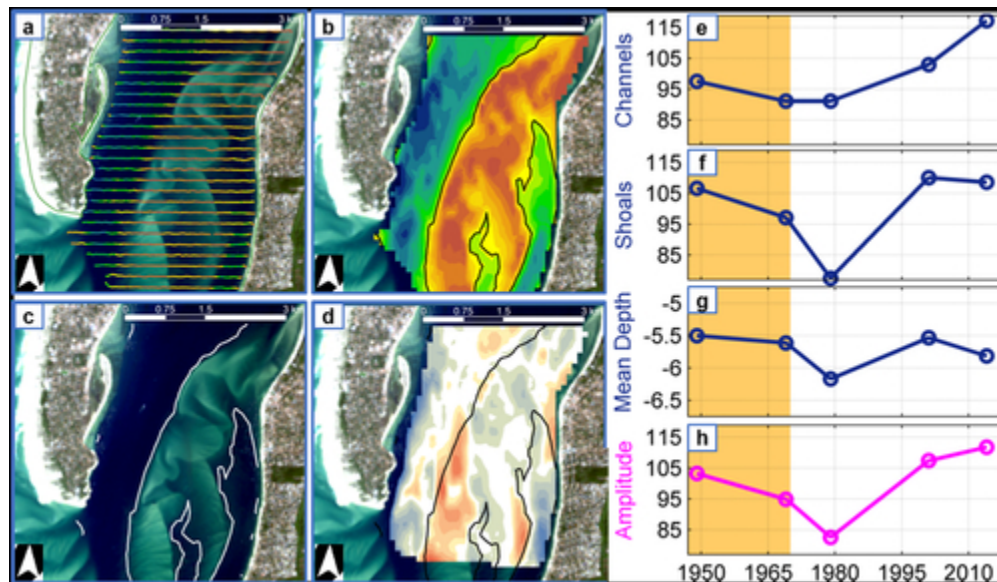
Measuring the spit's extension relative to the position of Cap Ferret's lighthouse. **Upper panels:** charts and coastlines from 1768 and 1826 and Satellite Landsat 8 image from October 2014, red dotted lines represent the 2014 coastline and the red stars indicate the lighthouse's position, white dashed lines materialize the axe onto which spit-end positions were orthogonally projected and measured, the black sector in the right panel represents the spit-end migration range; **lower panel:** the grey curve shows the spit-end path between 1768 and 1936, grey error bars stand for historical charts and the black ones for modern charts, asterisk symbol stand for spit-end positions in Figure 2**b-e**.

42x28mm (300 x 300 DPI)



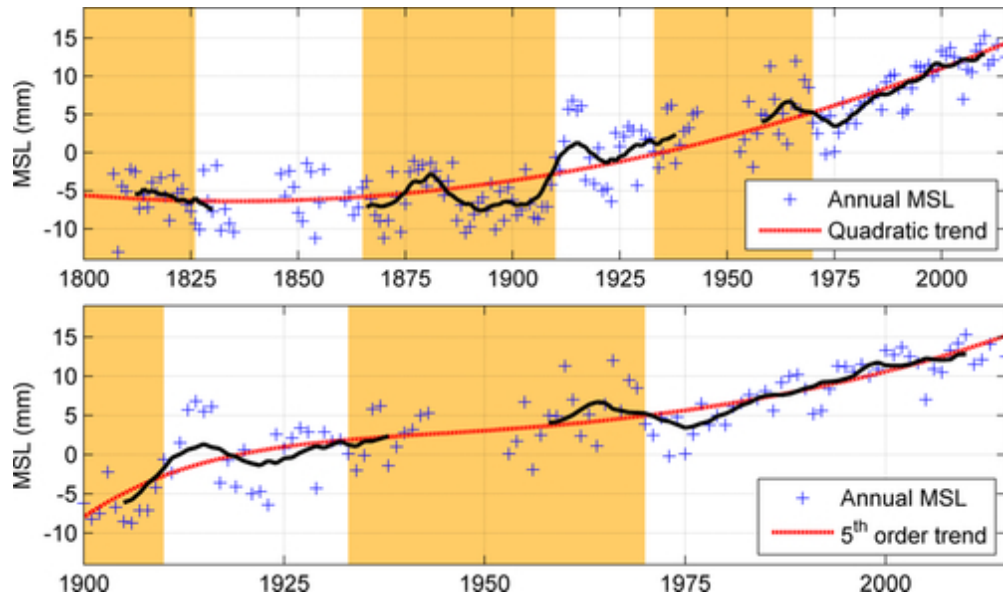
Positions of the Cap Ferret spit-end measured on aerial photographs. **Upper panels:** series of aerial photographs of the spit-end, red dotted lines represent the 2014 coastline, black asterisk symbols materialize the spit-end positions for the given years, superimposed on photographs from 1934 and 1946 are the shorelines reproduced from charts of 1932 and 1936 respectively; **lower panel:** distance of the spit-end to lighthouse's position, black asterisk symbols correspond to those on the upper panel.

42x19mm (300 x 300 DPI)



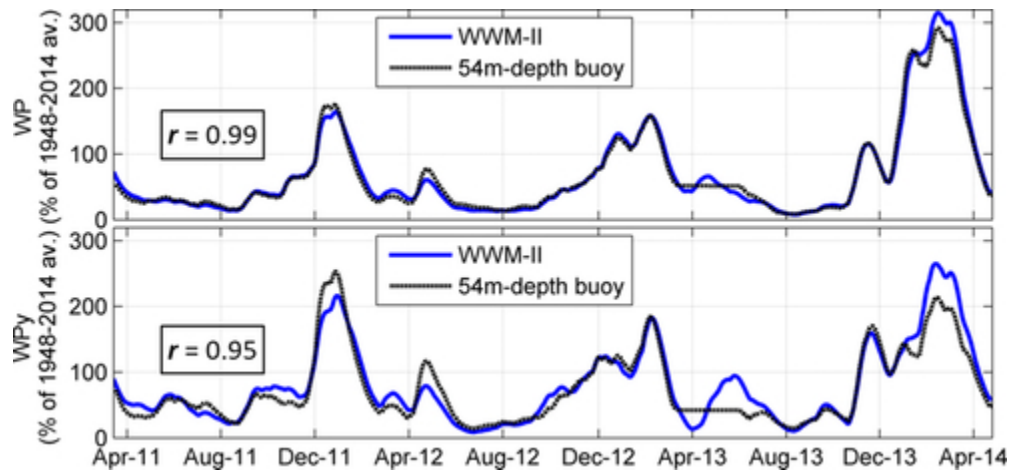
Inlet throat bathymetric data. **a)** summer 2014 along transect soundings; **b)** interpolated bathymetry with the -7 m NGF contours (black lines); **c)** -7 m NGF contours superimposed onto October 2014 Landsat image; **d)** erosion (blue) – deposition (red) patterns over the 12.74 km² area covered by all 5 surveys between 1949 and 2014; **e-h)** channel volume (below -7 m NGF), shoal volume (above -7 m NGF), overlapping area mean depth (m NGF) and inlet morphological amplitude over panel **d)**'s area (**e,f** and **h** are in percent of averaged values for all 5 surveys).

42x24mm (300 x 300 DPI)



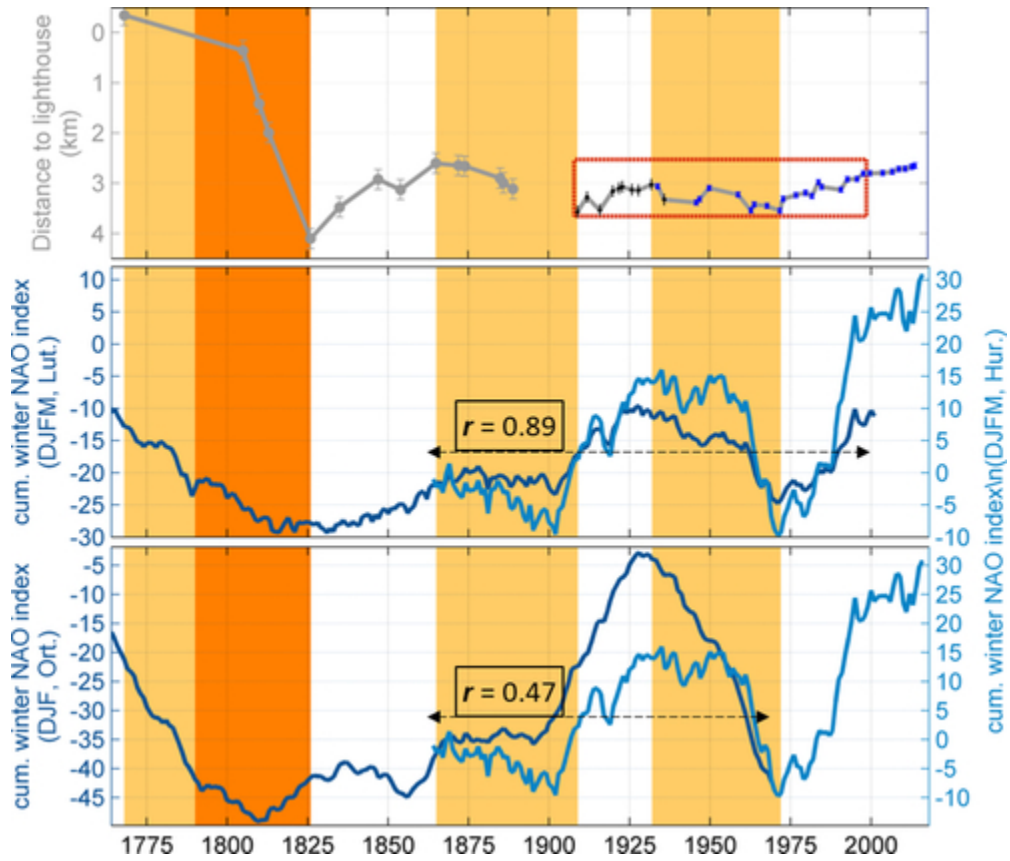
Brest tidal gauge Mean Sea Level (MSL) variation. **Upper panel:** annual MSL data from 1807 to 2015 recovered from the PMSL observatory (Holgate et al., 2013), black lines are the 11-year centred running mean of annual measurements and the thick dotted red line is the quadratic fit of all the data; **lower panel:** same as above with data from 20th century onward fitted with a 5th order polynomial function.

42x24mm (300 x 300 DPI)



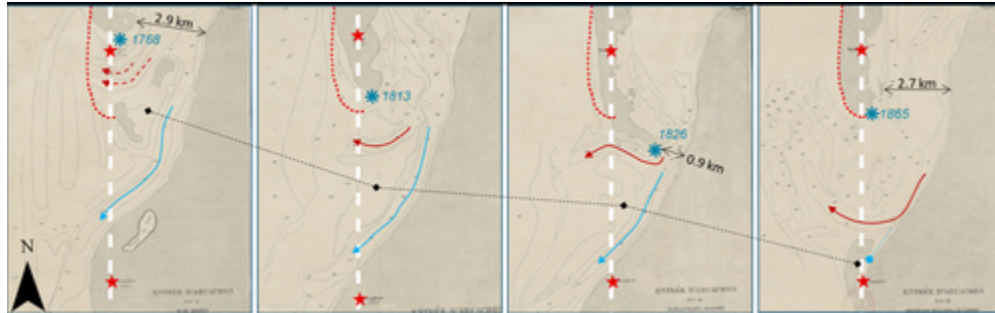
Local, 54 m water depth wave hindcast. **Upper panel:** 90-day running mean of the wave power (WP; linear wave theory approximation) 15 km offshore Cap Ferret, solid blue line are wind wave model (WWM-II, Roland et al., 2012) results with Bertin et al. (2015) setup, dotted black line are the wave buoy observations (CETMEF, n.d.) between April 2011 and May 2014, data is normalized using mean WP value over the hindcast period (1948-2014); **lower panel:** same as above with the alongshore component of the wave power (WP_y); *r* values are Pearson's linear correlation coefficients between plotted curves.

42x19mm (300 x 300 DPI)



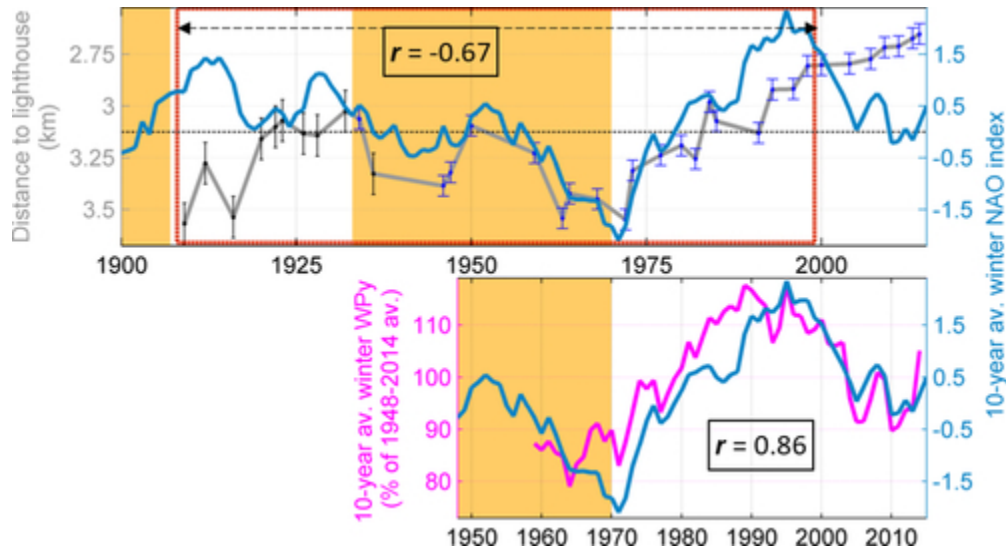
Spit-end path and cumulated winter NAO indices between 1768 and 2014. **Upper panel:** the grey curve shows the distance from the spit-end to the Cap Ferret lighthouse as on Figures 3&4 (red dotted frame is for next Figure 8's zoom); **mid panel:** darker blue curve is the cumulated winter (DJFM) index of the NAO reconstruction of Luterbacher et al. (1999), lighter blue curve is the same but for (Hurrell's (2015) station-based (DJFM) index; **lower panel:** darker blue curve is the cumulated winter (DJF) index of the NAO reconstruction of Ortega et al. (2015), lighter blue curve is the same but for Hurrell's (2015) station-based (DJFM) index; on all panels, orange shades indicate periods of spit elongation with the Dalton Minimum period in darker orange, r values are Pearson's linear correlation coefficients between plotted curves.

42x35mm (300 x 300 DPI)



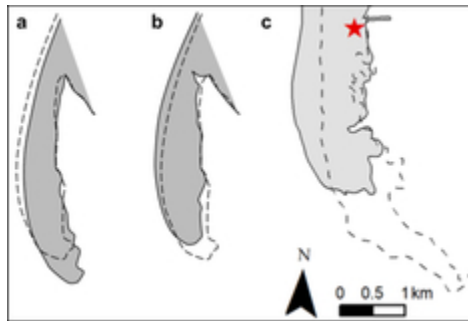
Evolution of the spit-inlet system across the Dalton Minimum (1780 – 1830). Navigation charts from years 1768, 1813, 1826 and 1865; blue asterisks indicate the positions of the spit terminus at the respective dates; black arrows materialize the inlet minimal width; red and blue arrows materialize the position of respectively the northern and southern channels; the dotted black line depicts the migration of the main inlet shoal barycentre; common red stars, dotted white axis and dotted red line are the same as in Figures 2 and 3.

42x13mm (300 x 300 DPI)



NAO relationships with Cap Ferret’s spit-end and local wave climate. **Upper panel:** in grey is the path of the spit-end, as the distance from the spit-end to the Cap Ferret lighthouse, as on Figures 3&4 and over since 1909, superimposed blue curve is Hurrell’s (2015) station-based NAO winter index, averaged of 10 years preceding each observation; **lower panel:** same winter NAO index curve as above, along with hindcasted alongshore winter wave power (WPy), averaged in same fashion as the NAO index and normalized using mean WPy value over the hindcast period (1948-2014); on both panels, orange shades indicate periods of spit elongation, *r* values are Pearson’s linear correlation coefficients between plotted curves.

42x22mm (300 x 300 DPI)



Sandspit's morphological response to changes in mean wave direction. **a**) spit-end response to a decrease of the averaged wave angle of incidence, modelled by (and reproduced from) Ashton et al. (2016), dashed line represents initial shoreline and shaded area represents the spit-end contours after waves became more shore normal; **b**) same as panel **a**, but for an increase of the averaged wave angle of incidence, or after waves became more oblique; **c**) dashed line represents Cap Ferret spit-end in 1826, at the end of the Dalton Minimum, and shaded area represents the spit-end in 1865.

19x13mm (300 x 300 DPI)